J. Fluid Mech. (1988), *vol.* 197, *pp.* 1–37
Printed in Great Britain

A strong-interaction theory for the motion of arbitrary three-dimensional clusters of spherical particles at low Reynolds number

By QAIZAR HASSONJEE,† PETER GANATOS‡ AND ROBERT PFEFFER‡

†Spraylat Corporation, 716 S. Columbus Ave., Mt. Vernon, NY 10550, USA
‡The City College of The City University of New York, New York, NY 10031, USA

(Received 29 July 1987 and in revised form 28 April 1988)

This paper contains an 'exact' solution for the hydrodynamic interaction of a three-dimensional finite cluster at arbitrarily sized spherical particles at low Reynolds number. The theory developed is the most general solution to the problem of an assemblage of spheres in a three-dimensional unbounded media. The boundary-collocation truncated-series solution technique of Ganatos, Pfeffer & Weinbaum (1978) for treating planar symmetric Stokes flow problems has been extensively modified to treat the non-symmetric multibody problem. The orthogonality properties of the eigenfunctions in the azimuthal direction are used to satisfy the no-slip boundary conditions exactly on entire rings on the surface of each particle rather than just at discrete points.

Detailed comparisons with the exact bipolar solutions for two spheres show the present theory to be accurate to five significant figures in predicting the translational and angular velocity components of the particles at all orientations for interparticle gap widths as close as 0.1 particle diameter. Convergence of the results to the exact solution is rapid and systematic even for unequal-sized spheres ($a_1/a_2 = 2$). Solutions are presented for several interesting and intriguing configurations involving three or more spherical particles settling freely under gravity in an unbounded fluid or in the presence of other rigidly held particles. Advantage of symmetry about the origin is taken for symmetric configurations to reduce the collocation matrix size by a factor of 64. Solutions for the force and torque on three-dimensional clusters of up to 64 particles have been obtained, demonstrating the multiparticle interaction effects that arise which would not be present if only pair interactions of the particles were considered. The method has the advantage of yielding a rather simple expression for the fluid velocity field which is of significance in the treatment of convective heat and mass transport problems in multiparticle systems.

1. Introduction

The slow motion of particles in an incompressible Newtonian fluid occurs in many physical processes and therefore the study of this problem is important both from a practical and theoretical point of view. Some important processes that depend on the relative motion of a suspension of particles include the mass transfer around a cluster of spheres falling in a viscous fluid, modelling of packed- and fluidized-bed reactors and filters, predicting the efficiency of spray scrubber devices, determining the agglomeration rate of aerosol particles in the atmosphere, the motion of red cells in

the microcirculation and the transport of vesicles across the endothelial cell layer lining the artery wall.

As detailed in this section, the only solutions that are currently available in the literature for the hydrodynamic interaction of spherical particles are: flow past two identical (Goldman, Cox & Brenner 1966; Kim & Mifflin 1985) or unequal spheres (Davis 1969) at an arbitrary orientation, a first-order weak-interaction theory for the three-dimensional multisphere problem (Hocking 1964), quasi-steady time-dependent motion of three or more spheres settling under gravity in vertical planar configurations (Ganatos, Pfeffer & Weinbaum 1978) and the drag force on three-dimensional periodic arrays (Zick & Homsy 1982; Sangani & Acrivos 1982). Recently, Durlofsky, Brady & Bossis (1987) have developed a theory equivalent to the method of reflections for predicting the velocity and force on a three-dimensional assemblage of spheres. However no exact interaction theory exists for non-symmetric three-dimensional multiparticle configurations involving a finite number of particles.

The existence of a bispherical coordinate system has enabled exact solutions to be obtained for a variety of problems involving two spherical particles. Stimson & Jeffrey (1926) considered the axisymmetric motion of two spheres. The asymmetric case of motion perpendicular to the line of centres was treated by Dean & O'Neill (1963). Further extensions of this problem have been reported by Goldman *et al.* (1966) and Wakiya (1967) for the slow motion of two identical arbitrarily oriented spheres, by Kim & Mifflin (1985) for the complete solution of the motion of two equal spheres and by Davis (1969) for the case of two unequal spheres slowly rotating or translating perpendicular to their line of centres. Wacholder & Sather (1974) used the method of reflections to obtain the solution for two unequal spheres settling under gravity in a quiescent fluid.

Theoretical solutions for predicting the drag force on a periodic array of spheres are currently available in the literature. Hasimoto (1959) developed a perturbation solution for multiparticle systems to obtain the drag on each sphere in terms of an expansion in fractional powers of the concentration of the packing. He derived the periodic fundamental solution of the creeping motion equations and after expanding the velocity profile in terms of the fundamental solution and its derivatives, obtained an expression for the drag force for cubic arrays. However this method could be used only for dilute packing. Sangani & Acrivos (1982) extended Hasimoto's method to calculate the drag to $O(c^3)$ for cubic and hexagonal arrays of spheres, where c is the volume fraction of the spheres. They derived an expression for the dimensionless drag to $O(c^{10})$ for arrays of spheres packed in simple cubic, body-centred cubic and face-centred cubic lattices. Using the boundary-integral method, Zick & Homsy (1982) formulated the problem for flow past three-dimensional periodic arrays of spheres as a set of two-dimensional integral equations for the unknown surface stress distribution, and obtained the drag force exerted on each sphere as a function of particle concentration and type of packing.

The method of reflections has been used by many investigators to study multiparticle interactions for a finite number of spheres (Happel & Brenner 1973). The technique is good only for weak interactions where the particles are spaced far apart and exhibits poor convergence characteristics for concentrated systems. Hocking (1964) used a single reflection to describe the particle interactions for a cluster of spheres falling in a viscous fluid neglecting inertial effects and assuming that the distance between any two spheres is large compared with their radii. He examined the stability of steady configurations for 3, 4, 5 and 6 spheres forming

regular polygons and compared his results with the experimental observations for the same motion reported by Jayaweera, Mason & Slack (1964).

Most recently, Durlofsky, Brady & Bossis (1987) have developed a simulation method capable of computing static and dynamic properties of a finite system of hydrodynamically interacting spherical particles. The method uses an integral representation for the velocity field at any point in the fluid in Stokes flow in terms of a multipole expansion, in conjunction with the Faxén formulae for the motion of a sphere immersed in a flow field, to form the mobility matrix. The mobility matrix is inverted to obtain the resistance matrix. The inversion of the mobility matrix introduces the many-body resistance interactions. The lubrication effect is added to the resistance matrix in a pairwise additive manner using the exact two-sphere resistance interaction functions. Particle velocities are then determined by solving the matrix equation. The method has the advantage of yielding the instantaneous particle velocities with minimal computational effort thus allowing quasi-steady time-dependent calculations to be performed for determining the particle trajectories. However the method is not exact and does not readily permit the evaluation of the local fluid velocity field.

Gluckman, Pfeffer & Weinbaum (1971) have obtained exact Stokes solutions for flow past a finite line array of spheres or spheroids by placing an infinite series of appropriate singularities at the origin of each sphere or spheroid. This study has shown that it is most efficient to use a truncated series of point singularities and satisfy boundary conditions at discrete points on each object simultaneously. This method, the boundary-collocation, truncated-series solution technique, yields first-, second-, and fifth-order truncation solutions for the drag which are accurate to 2.5, 0.1 and 0.001 % respectively for the flow parallel to the axis of two touching spheres. This rapid convergence is in sharp contrast to the slowly converging results obtained using the method of reflections. The theory was applied to treat flow past an arbitrary convex body of revolution in Gluckman, Weinbaum & Pfeffer (1972) and two unequal spheres or spheroids (Liao & Kreuger 1980). Ganatos *et al.* (1978) made major modifications to the theory and applied it to three-dimensional flows with planar symmetry. This theory has been used to obtain the quasi-steady time-dependent motion of three or more spheres settling under gravity in vertical planar configurations. The theory has also been extended to bounded flow problems such as the motion of a sphere of arbitrary size and position between two planar parallel walls (Ganatos, Weinbaum & Pfeffer 1980*a*; Ganatos, Pfeffer & Weinbaum 1980*b*; Ganatos, Weinbaum & Pfeffer 1982). Most recently the theory has been used in conjunction with the boundary-integral method to treat the off-axis approach of a spherical particle to a circular orifice (Yan *et al.* 1987).

The collocation technique of Ganatos *et al.* (1978) has certain restrictions and difficulties. The method uses collocation points to satisfy the no-slip boundary conditions on the surface of each sphere and is restricted to planar configurations. The error in drag force for arbitrary settling of two spheres at a spacing of 1.128 diameters was 4% and the error in the much smaller horizontal drift velocity and angular velocities was as much as 20%. Using additional boundary collocation points did not always produce better accuracy for all orientations. The most important shortcoming of this technique was the selection of boundary points; a different set of boundary points should be used for each orientation to give the best accuracy. About 6000 test solutions showed that, while a given configuration of points produced good results over a certain range of orientations, the same set of points could produce substantial errors outside this range.

The purpose of this paper is two-fold. First, we wish to present a fundamental theory for evaluating the hydrodynamic interactions of unrestricted three-dimensional finite multiparticle configurations. Secondly, we wish to modify the existing boundary-collocation theory developed by Ganatos *et al.* (1978) for systems of particles in planar configurations to eliminate the convergence difficulties that were encountered. This paper is presented in six sections. Section 2 details the general formulation of the collocation technique for an arbitrary configuration of J spheres. Section 3 shows the strength of the method in duplicating the exact solutions for two spheres spaced as close as 1.12 diameters at any orientation. Section 4 demonstrates the ability of this technique to handle arbitrary three-dimensional multisphere configurations. Some multisphere steady configurations falling under gravity are studied. Results are presented for an intriguing three sphere L-shaped configuration in which the method of paired interactions fails to predict the lateral motion of the corner sphere in that configuration. Solutions for the fluid velocity field through a configuration of three spheres arranged in an equilateral triangle are presented showing the development of separated regions of closed streamlines for certain orientations of the configuration. In §5 advantage of symmetry is used to reduce the collocation matrix by a factor of 64 to obtain the drag and torque on clusters of 8, 16, 24, 32, 48, 56 and 64 spheres. Finally §6 discusses the strengths and weaknesses of this method and its future use for obtaining solutions of other fluid-mechanics problems.

2. Formulation

Consider the slow motion of J spheres (identical or unequal) moving in a viscous fluid in an arbitrary three-dimensional configuration as shown in figure 1. The flow field satisfies the creeping motion equations:

$$\mu\nabla^2 \boldsymbol{V} = \nabla P, \quad \nabla\cdot\boldsymbol{V} = 0. \tag{2.1a, b}$$

The fundamental solution of (2.1a, b) that is capable of describing an arbitrary disturbance on the surface of a sphere of radius a was obtained by Lamb (1945) and given by Happel & Brenner (1973, p. 65) as

$$\boldsymbol{V} = \sum_{n=1}^{\infty} [\nabla\times(\boldsymbol{r}\chi_{-(n+1)}) + \nabla\Phi_{-(n+1)} - \frac{(n-2)}{\mu(2n-1)\,2n} r^2\nabla P_{-(n+1)} + \frac{(n+1)}{\mu n(2n+1)}\boldsymbol{r}P_{-(n+1)}]. \tag{2.2}$$

Here $\chi_{-(n+1)}$, $\Phi_{-(n+1)}$ and $P_{-(n+1)}$ are solid spherical harmonic functions of order $-(n+1)$ and $\boldsymbol{r}$ is the radial position vector whose origin is at the centre of the sphere.

For J spheres moving slowly in an unbounded, incompressible, Newtonian, quiescent fluid, the linear superposition of J individual spherical solutions yields

$$\boldsymbol{V} = \sum_{j=1}^{J}\sum_{n=1}^{\infty} [\nabla\times(\boldsymbol{r}_j\chi_{-(n+1),j}) + \nabla\Phi_{-(n+1),j} - \frac{(n-2)}{\mu(2n-1)\,2n} r_j^2\nabla P_{-(n+1),j} + \frac{(n+1)}{\mu n(2n+1)}\boldsymbol{r}_j P_{-(n+1),j}], \tag{2.3}$$

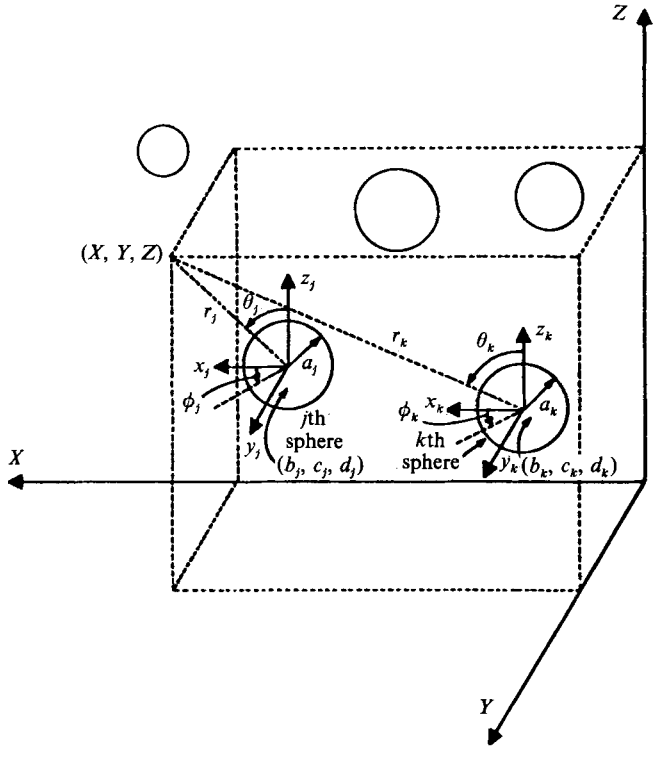

FIGURE 1. Geometry for system of spheres falling freely in the three-dimensional space.

where $\chi_{-(n+1),j}$ $\Phi_{-(n+1),j}$ and $P_{-(n+1),j}$ are solid spherical harmonic functions of order $-(n+1)$ which depend on r_j, θ_j and ϕ_j, the stationary spherical coordinates measured from the centre of the jth sphere at the instant of time under consideration.

In general, the three solid spherical harmonic functions in (2.3) have the following form:

$$\begin{bmatrix} \chi_{-(n+1),j} \\ \phi_{-(n+1),j} \\ P_{-(n+1),j} \end{bmatrix} = \sum_{m=0}^{\infty} P_n^m(\xi_j) \frac{1}{r_j^{n+1}} \left\{ \begin{bmatrix} A_{jmn} \\ C_{jmn} \\ E_{jmn} \end{bmatrix} \sin m\phi_j + \begin{bmatrix} B_{jmn} \\ D_{jmn} \\ F_{jmn} \end{bmatrix} \cos m\phi_j \right\}, \tag{2.4}$$

where $P_n^m(\xi_j)$ is the associated Legrandre function, $\xi_j = \cos\theta_j$ and $A_{jmn}, \ldots, F_{jmn}$ are unknown constants, which for a given configuration of particles are determined by satisfying the no-slip boundary conditions on the surface of each particle.

Substituting (2.4) into (2.3) an expression for the fluid velocity field is obtained:

$$\boldsymbol{V} = \sum_{j=1}^{J} \sum_{n=1}^{\infty} \sum_{m=0}^{n} [V_{r_j}(r_j, \theta_j, \phi_j)\, \hat{\boldsymbol{e}}_{r_j} + V_{\theta_j}(r_j, \theta_j, \phi_j)\, \hat{\boldsymbol{e}}_{\theta_j} + V_{\phi_j}(r_j, \theta_j, \phi_j)\, \hat{\boldsymbol{e}}_{\phi_j}], \tag{2.5}$$

where the velocity components V_{r_j}, V_{θ_j} and V_{ϕ_j} are given by

$$V_{r_j} = -\frac{(n+1)}{r_j^{(n+2)}} P_n^m(\xi_j)\,(C_{jmn} \cos m\phi_j + D_{jmn} \sin m\phi_j)$$

$$+ \frac{(n+1)}{2\mu(2n-1)} \frac{P_n^m(\xi_j)}{r_j^n} (E_{jmn} \cos m\phi_j + F_{jmn} \sin m\phi_j), \tag{2.6a}$$

$$V_{\theta_j} = -\frac{m}{\sin\theta_j\, r_j^{(n+1)}} P_n^m(\xi_j)\,(A_{jmn}\sin m\phi_j - B_{jmn}\cos m\phi_j)$$
$$-\frac{\sin\theta_j}{r_j^{(n+2)}}\frac{\mathrm{d}P_n^m(\xi_j)}{\mathrm{d}\xi_j}(C_{jmn}\cos m\phi_j + D_{jmn}\sin m\phi_j)$$
$$+\frac{(n-2)\sin\theta_j}{2n\mu(2n-1)\, r_j^n}\frac{\mathrm{d}P_n^m(\xi_j)}{\mathrm{d}\xi_j}(E_{jmn}\cos m\phi_j + F_{jmn}\sin m\phi_j), \tag{2.6b}$$

$$V_{\phi_j} = \frac{\sin\theta_j}{r_j^{(n+1)}}\frac{\mathrm{d}P_n^m(\xi_j)}{\mathrm{d}\xi_j}(A_{jmn}\cos m\phi_j + B_{jmn}\sin m\phi_j)$$
$$-\frac{m}{\sin\theta_j\, r_j^{(n+2)}} P_n^m(\xi_j)\,(C_{jmn}\sin m\phi_j - D_{jmn}\cos m\phi_j)$$
$$+\frac{(n-2)\, mP_n^m(\xi)}{2n\mu(2n-1)\sin\theta_j\, r_j^n}(E_{jmn}\sin m\phi_j + F_{jmn}\cos m\phi_j). \tag{2.6c}$$

The spherical coordinates (r_j, θ_j, ϕ_j) and their unit vectors $(\hat{\boldsymbol{e}}_{r_j}, \hat{\boldsymbol{e}}_{\theta_j}, \hat{\boldsymbol{e}}_{\phi_j})$ originate from the centre of each sphere and so they are different for each sphere. It is thus necessary to perform a transformation of coordinates to express the fluid velocity field in terms of a single orthogonal coordinate system. To facilitate applying the no-slip boundary conditions on the surface of each sphere, it is convenient to express all the coordinates in terms of a single spherical coordinate system whose origin lies at the centre of the kth sphere. If the origin of the kth sphere is at the point (b_k, c_k, d_k) in a global Cartesian coordinate system (X, Y, Z) (see figure 1) and the origin of the jth sphere is (b_j, c_j, d_j), the spherical coordinates of an arbitrary point in space relative to the jth sphere are related to the spherical coordinates of the point relative to the kth sphere by the relations

$$r_j^2 = 2r_k[\sin\theta_k\cos\phi_k\, b_{kj} + \sin\theta_k\sin\phi_k\, c_{kj} + \cos\theta_k\, d_{kj}] + r_k^2 + b_{kj}^2 + c_{kj}^2 + d_{kj}^2, \tag{2.7a}$$

$$\theta_j = \tan^{-1}\left[\frac{r_k^2\sin^2\theta_k + b_{kj}^2 + c_{kj}^2 + 2r_k\sin\theta_k(\cos\theta_k\, b_{kj} + \sin\phi_k\, c_{kj})}{(r_k\cos\theta_k\, d_{kj})}\right], \tag{2.7b}$$

$$\phi_j = \tan^{-1}\left[\frac{r_k\sin\theta_k\sin\phi_k + c_{kj})}{r_k\sin\theta_k\cos\phi_k + b_{kj})}\right], \tag{2.7c}$$

where $$b_{kj} = b_k - b_j, \quad c_{kj} = c_k - c_j \quad \text{and} \quad d_{kj} = d_k - d_j.$$

Details of the derivation of these coordinate transformations are given in Appendix A. Care must be exercised in the use of (2.7c) to assure that the value of ϕ_j that is computed lies in the appropriate quadrant.

The unit vectors of the jth and kth spherical coordinate systems are related via the matrix equation:

$$\begin{bmatrix}\hat{\boldsymbol{e}}_{r_j}\\ \hat{\boldsymbol{e}}_{\theta_j}\\ \hat{\boldsymbol{e}}_{\phi_j}\end{bmatrix} = \begin{bmatrix} f_{1jk} & f_{2jk} & f_{3jk}\\ f_{4jk} & f_{5jk} & f_{6jk}\\ f_{7jk} & f_{8jk} & f_{9jk}\end{bmatrix}\begin{bmatrix}\hat{\boldsymbol{e}}_{r_k}\\ \hat{\boldsymbol{e}}_{\theta_k}\\ \hat{\boldsymbol{e}}_{\phi_k}\end{bmatrix}, \tag{2.8}$$

where

$$f_{1jk} = \sin\theta_j \sin\theta_k \cos(\phi_j - \phi_k) + \cos\theta_k \cos\theta_j, \tag{2.9a}$$

$$f_{2jk} = \sin\theta_j \cos\theta_k \cos(\phi_j - \phi_k) - \sin\theta_k \cos\theta_j, \tag{2.9b}$$

$$f_{3jk} = \sin\theta_j \sin(\phi_j - \phi_k), \tag{2.9c}$$

$$f_{4jk} = \cos\theta_j \sin\theta_k \cos(\phi_j - \phi_k) - \cos\theta_k \sin\theta_j, \tag{2.9d}$$

$$f_{5jk} = \cos\theta_j \cos\theta_k \cos(\phi_j - \phi_k) + \sin\theta_k \sin\theta_j, \tag{2.9e}$$

$$f_{6jk} = \cos\theta_j \sin(\phi_j - \phi_k), \tag{2.9f}$$

$$f_{7jk} = -\sin\theta_k \sin(\phi_j - \phi_k), \tag{2.9g}$$

$$f_{8jk} = -\cos\theta_k \sin(\phi_j - \theta_k), \tag{2.9h}$$

$$f_{9jk} = \cos(\phi_j - \phi_k). \tag{2.9i}$$

The derivation of (2.8) and (2.9) is also given in Appendix A. Here the angles θ_j and ϕ_j are related to the spherical coordinates (r_k, θ_k, ϕ_k) using (2.7).

Substituting (2.7), (2.8) and (2.9) into (2.5) and (2.6) yields an expression for the fluid velocity field in terms of the spherical coordinates (r_k, θ_k, ϕ_k) originating at the centre of the kth sphere which can be written in the following form:

$$\boldsymbol{V}_k = [V_{r_k}\hat{\boldsymbol{e}}_{r_k} + V_{\theta_k}\hat{\boldsymbol{e}}_{\theta_k} + V_{\phi_k}\hat{\boldsymbol{e}}_{\phi_k}], \tag{2.10}$$

where

$$V_{r_k} = \sum_{j=1}^{J}\sum_{n=1}^{\infty}\sum_{m=0}^{n}[A_{jmn}A'_{jkmn} + B_{jmn}B'_{jkmn} + \ldots + F_{jmn}F'_{jkmn}], \tag{2.11a}$$

$$V_{\theta_k} = \sum_{j=1}^{J}\sum_{n=1}^{\infty}\sum_{m=0}^{n}[A_{jmn}A''_{jkmn} + B_{jmn}B''_{jkmn} + \ldots + F_{jmn}F''_{jkmn}], \tag{2.11b}$$

$$V_{\phi_k} = \sum_{j=1}^{J}\sum_{n=1}^{\infty}\sum_{m=0}^{n}[A_{jmn}A'''_{jkmn} + B_{jmn}B'''_{jkmn} + \ldots + F_{jmn}F'''_{jkmn}]. \tag{2.11c}$$

Here $V_{r_k}, V_{\theta_k}, V_{\phi_k}$ are the fluid velocity components in a stationary spherical coordinate system whose origin lies at the centre of the kth sphere. The primed quantities in (2.11) are known functions of the coordinates r_k, θ_k and ϕ_k and are given in Appendix B. The unprimed coefficients are the unknown constants introduced in (2.4).

The 'no-slip' boundary conditions which must be satisfied on the surface of each sphere are

$$\boldsymbol{V}|_{r_k=a_k} = \boldsymbol{U}_k + \boldsymbol{\Omega}_k \times a_k\hat{\boldsymbol{e}}_{r_k}, \tag{2.12}$$

where a_k is the radius of the kth sphere and $\boldsymbol{U}_k$ and $\boldsymbol{\Omega}_k$ are the translational and rotational velocities of the kth sphere whose Cartesian components are denoted by

$$\boldsymbol{U}_k = U_k\hat{\boldsymbol{i}} + V_k\hat{\boldsymbol{j}} + W_k\hat{\boldsymbol{k}}, \tag{2.13}$$

$$\boldsymbol{\Omega}_k = (\Omega_x)_k\hat{\boldsymbol{i}} + (\Omega_y)_k\hat{\boldsymbol{j}} + (\Omega_z)_k\hat{\boldsymbol{k}}. \tag{2.14}$$

Substituting (2.13) and (2.14) into (2.12) and using (A 6) gives the three spherical components of velocity on the surface of the kth sphere as

$$V_{r_k}|_{r_k=a_k} = U_k \sin\theta_k \cos\phi_k + V_k \sin\theta_k \sin\phi_k + W_k \cos\theta_k, \tag{2.15a}$$

$$V_{\theta_k}|_{r_k=a_k} = U_k \cos\theta_k \cos\phi_k + V_k \cos\theta_k \sin\phi_k - W_k \sin\theta_k + a_k[(\Omega_y)_k \cos\theta_k - (\Omega_x)_k \sin\theta_k], \tag{2.15b}$$

$$V_{\phi_k}|_{r_k=a_k} = -U_k \sin\phi_k + V_k \cos\phi_k - a_k[((\Omega_x)_k \cos\phi_k + (\Omega_y)_k \sin\phi_k)\cos\theta_k - (\Omega_z)_k \sin\theta_k]. \tag{2.15c}$$

To enable application of the boundary conditions (2.15) on the surface of each sphere, the order of summation $\Sigma_{n=1}^{\infty}\Sigma_{m=0}^{n}$ in (2.11) is changed to

$$\sum_{m=0}^{\infty}\sum_{\substack{n=m\\ n\neq 0}}^{\infty}$$

without loss of any terms in the series and the term $j=k$ is extracted from the series $\Sigma_{j=1}^{J}$. Furthermore when $j=k$, the term $m=0$ is written separately. Evaluating (2.11) at $r_k=a_k$ and equating it to (2.15) gives

$$\begin{aligned}
V_{r_k}|_{r_k=a_k} &= U_k\sin\theta_k\cos\phi_k + V_k\sin\theta_k\sin\phi_k + W_k\cos\theta_k\\
&= \sum_{n=0}^{\infty}[A_{k0n}A'_{kk0n}+B_{k0n}B'_{kk0n}+\ldots+F_{k0n}F'_{kk0n}]\\
&\quad+\sum_{m=1}^{\infty}\sum_{n=m}^{\infty}[A_{kmn}A'_{kkmn}+B_{kmn}B'_{kkmn}+\ldots+F_{kmn}F'_{kkmn}]\\
&\quad+\sum_{\substack{j=1\\ j\neq k}}^{J}\sum_{m=0}^{\infty}\sum_{n=m}^{\infty}[A_{jmn}A'_{jkmn}+B_{jmn}B'_{jkmn}+\ldots+F_{jmn}F'_{jkmn}], \qquad (2.16a)\\
V_{\theta_k}|_{r_k=a_k} &= U_k\cos\theta_k\cos\phi_k + V_k\cos\theta_k\sin\phi_k - W_k\sin\theta_k\\
&\quad+a_k[(\Omega_y)_k\cos\theta_k-(\Omega_x)_k\sin\theta_k]\\
&= \sum_{n=0}^{\infty}[A_{k0n}A''_{kk0n}+B_{k0n}B''_{kk0n}+\ldots+F_{k0n}F''_{kk0n}]\\
&\quad+\sum_{m=1}^{\infty}\sum_{n=m}^{\infty}[A_{kmn}A''_{kkmn}+B_{kmn}B''_{kkmn}+\ldots+F_{kmn}F''_{kkmn}]\\
&\quad+\sum_{\substack{j=1\\ j\neq k}}^{J}\sum_{m=0}^{\infty}\sum_{n=m}^{\infty}[A_{jmn}A''_{jkmn}+B_{jmn}B''_{jkmn}+\ldots+F_{jmn}F''_{jkmn}], \qquad 6b)\\
V_{\phi_k}|_{r_k=a_k} &= U_k\sin\phi_k + V_k\cos\phi_k\\
&\quad-a_k[((\Omega_x)_k\cos\phi_k+(\Omega_y)_k\sin\phi_k)\cos\theta_k-(\Omega_z)_k\sin\theta_k]\\
&= \sum_{n=0}^{\infty}[A_{k0n}A'''_{kk0n}+B_{k0n}B'''_{kk0n}+\ldots+F_{k0n}F'''_{kk0n}]\\
&\quad+\sum_{m=1}^{\infty}\sum_{n=m}^{\infty}[A_{kmn}A'''_{kkmn}+B_{kmn}B'''_{kkmn}+\ldots+F_{kmn}F'''_{kkmn}]\\
&\quad+\sum_{\substack{j=1\\ j\neq k}}^{J}\sum_{m=0}^{\infty}\sum_{n=m}^{\infty}[A_{jmn}A'''_{jkmn}+B_{jmn}B'''_{jkmn}+\ldots+F_{jmn}F'''_{jkmn}], \qquad (2.16c)
\end{aligned}$$

where the primed functions depend only on the coordinates θ_k and ϕ_k and are given by (B 1)–(B 18) with $r_k=a_k$.

The terms $j=k$ in (2.16) (see Appendix B) depend only on the eigenfunctions $\sin m\phi_k$ and $\cos m\phi_k$ or are independent of ϕ_k. Thus these functions can be written in the form of a Fourier series in ϕ_k as

$$A'_0(\theta_k)+\sum_{m=1}^{\infty}[A'_m(\theta_k)\cos m\phi_k+B'_m(\theta_k)\sin m\phi_k]=F'(\theta_k,\phi_k), \qquad (2.17a)$$

$$A''_0(\theta_k)+\sum_{m=1}^{\infty}[A''_m(\theta_k)\cos m\phi_k+B''_m(\theta_k)\sin m\phi_k]=F''(\theta_k,\phi_k). \qquad (2.17b)$$

$$A'''_0(\theta_k)+\sum_{m=1}^{\infty}[A'''_m(\theta_k)\cos m\phi_k+B'''_m(\theta_k)\sin m\phi_k]=F'''(\theta_k,\phi_k). \qquad (2.17c)$$

Here the primed A, B and F functions depend only on the variables indicated and the unknown constants $A_{kmn}-F_{kmn}$ and are given in Appendix C. Multiplying (2.17) by the eigenfunction set $\{1, \cos m'\phi_k, \sin m'\phi_k\}$, integrating with respect to ϕ_k from 0 to 2π and utilizing the orthogonality properties of these eigenfunctions in this interval allows one to obtain explicit expressions for the primed A and B coefficients appearing in (2.17) and the unknown constants $A_{jmn}-F_{jmn}$ in (2.4). The results are:

for the r-component of velocity:

$$A'_0(\theta_k) = W_k \cos\theta_k - \frac{1}{2\pi}\int_0^{2\pi} \Sigma\,[A_{jmn}A'_{jkmn}+\ldots+F_{jmn}F'_{jkmn}]\,\mathrm{d}\phi_k, \tag{2.18a}$$

$$\begin{bmatrix} A'_1(\theta_k) \\ B'_1(\theta_k) \end{bmatrix} = \begin{bmatrix} U_k \\ V_k \end{bmatrix} \sin\theta_k - \frac{1}{\pi}\int_0^{2\pi} \Sigma\,[A_{jmn}A'_{jkmn}+\ldots+F_{jmn}F'_{jkmn}] \begin{bmatrix} \cos\phi_k \\ \sin\phi_k \end{bmatrix} \mathrm{d}\phi_k, \tag{2.18b, c}$$

$$\begin{bmatrix} A'_{m'}(\theta_k) \\ B'_{m'}(\theta_k) \end{bmatrix} = -\frac{1}{\pi}\int_0^{2\pi} \Sigma\,[A_{jmn}A'_{jkmn}+\ldots+F_{jmn}F'_{jkmn}] \begin{bmatrix} \cos m'\phi_k \\ \sin m'\phi_k \end{bmatrix} \mathrm{d}\phi_k, \quad m' > 1; \tag{2.18d, e}$$

for the θ-component of velocity:

$$A''_0(\theta_k) = -W_k \sin\theta_k - \frac{1}{2\pi}\int_0^{2\pi} \Sigma\,[A_{jmn}A''_{jkmn}+\ldots+F_{jmn}F''_{jkmn}]\,\mathrm{d}\phi_k, \tag{2.18f}$$

$$\begin{bmatrix} A''_1(\theta_k) \\ B''_1(\theta_k) \end{bmatrix} = \begin{bmatrix} V_k \\ -U_k \end{bmatrix} \cos\theta_k + a_k \begin{bmatrix} (\Omega_y)_k \\ -(\Omega_x)_k \end{bmatrix} - \frac{1}{\pi}\int_0^{2\pi} \Sigma\,[A_{jmn}A''_{jkmn}+\ldots + F_{jmn}F''_{jkmn}] \begin{bmatrix} \cos\phi_k \\ \sin\phi_k \end{bmatrix} \mathrm{d}\phi_k, \tag{2.18g, h}$$

$$\begin{bmatrix} A''_{m'}(\theta_k) \\ B''_{m'}(\theta_k) \end{bmatrix} = -\frac{1}{\pi}\int_0^{2\pi} \Sigma\,[A_{jmn}A''_{jkmn}+\ldots+F_{jmn}F''_{jkmn}] \begin{bmatrix} \cos m'\phi_k \\ \sin m'\phi_k \end{bmatrix} \mathrm{d}\phi_k, \quad m' > 1; \tag{2.18i, j}$$

for the ϕ-component of velocity:

$$A'''_0(\theta_k) = a_k(\Omega_z)_k \sin\theta_k - \frac{1}{2\pi}\int_0^{2\pi} \Sigma\,[A_{jmn}A'''_{jkmn}+\ldots+F_{jmn}F'''_{jkmn}]\,\mathrm{d}\phi_k, \tag{2.18k}$$

$$\begin{bmatrix} A'''_1(\theta_k) \\ B'''_1(\theta_k) \end{bmatrix} = \begin{bmatrix} V_k \\ -U_k \end{bmatrix} - a_k \begin{bmatrix} (\Omega_x)_k \\ (\Omega_y)_k \end{bmatrix} \cos\theta_k - \frac{1}{\pi}\int_0^{2\pi} \Sigma\,[A_{jmn}A'''_{jkmn}+\ldots + F_{jmn}F'''_{jkmn}] \begin{bmatrix} \cos\phi_k \\ \sin\phi_k \end{bmatrix} \mathrm{d}\phi_k, \tag{2.18l, n}$$

$$\begin{bmatrix} A'''_{m'}(\theta_k) \\ B'''_{m'}(\theta_k) \end{bmatrix} = -\frac{1}{\pi}\int_0^{2\pi} \Sigma\,[A_{jmn}A'''_{jkmn}+\ldots+F_{jmn}F'''_{jkmn}] \begin{bmatrix} \cos m'\phi_k \\ \sin m'\phi_k \end{bmatrix} \mathrm{d}\phi_k, \quad m' > 1; \tag{2.18n, o}$$

where Σ denotes $\sum_{\substack{j=1 \\ j\neq k}}^{J} \sum_{m=0}^{\infty} \sum_{n=m}^{\infty}$

and the functions $(A'_0 \dots B'''_{m'})$ on the left-hand side of (2.18) are given by (C 1)–(C 30) with m replaced by m'. The primed coefficients of the unknown constants on the right-hand side of (2.18) are given by (B 1)–(B 18) evaluated at $r_k = a_k$. The integrals appearing in (2.18) must be evaluated numerically.

We first consider the resistance problem in which the translation and angular velocity of each particle is prescribed and we seek to determine the force and torque acting on each particle to maintain this motion. The unknown constants $A_{jmn} - F_{jmn}$ introduced in (2.4) can be computed to any desired degree of accuracy from (2.18) and (C 1) to (C 30) by satisfying the no-slip boundary conditions on rings along the surface of each sphere as follows. The infinite series $\Sigma_{m=0}^{\infty}$ appearing in (2.18) is truncated after M terms to $\Sigma_{m=0}^{M-1}$. Furthermore the infinite series $\Sigma_{n=m}^{\infty}$ appearing in (2.18) and (C 1)–(C 3), (C 11)–(C 13) and (C 21)–(C 23) are each truncated after N terms to $\Sigma_{n=m}^{m+N}$. Since there are six sets of unknown constants A_{jmn}–F_{jmn}, for J spheres, this leaves a total of $6JMN$ unknown constants to be determined. However when $m = 0$ the coefficients of the constants B_{j0n}, D_{j0n} and F_{j0n} are identically zero for all three velocity components. Thus these three sets of constants do not appear in the final solution and the number of unknowns is reduced by $3JN$ to a total of $6JMN - 3JN$ or more simply, $3JN(2M-1)$.

To generate the equations needed to evaluate these unknown constants, the no-slip boundary conditions are satisfied at N discrete values of θ_k (rings) on the surface of each of the J spheres. We observe that for $m' = 0$, (2.18a, f, k) represent a total of $3JN$ equations. Similarly for $m' = 1$, (2.18b, c, g, h, l, m) are another $6JN$ equations. Finally, for $m' = 2, 3, 4 \dots M-1$ (2.18d, e, i, j, n, o) give an additional $6JN(M-2)$ equations. Thus from (2.18) we have a grand total of $3JN + 6JN + 6JN(M-2) = 3JN(2M-1)$ equations, which is exactly equal to the number of unknown constants. These equations may be solved using any standard linear matrix reduction technique.

The hydrodynamic force and torque acting on the jth particle is given by Happel & Brenner (1973) as

$$\boldsymbol{F}_j = -4\pi \boldsymbol{\nabla}(r_j^3 P_{-2,j}), \tag{2.19a}$$

$$\boldsymbol{T}_j = -8\pi \boldsymbol{\nabla}(r_j^3 \chi_{-2,j}). \tag{2.19b}$$

Using (2.4), the Cartesian components of the force and torque exerted by the fluid on each particle is given by

$$\boldsymbol{F}_j = -4\pi[E_{j11}\,\boldsymbol{i} + F_{j111}\boldsymbol{j} + E_{j01}\,\boldsymbol{k}], \tag{2.20a}$$

$$\boldsymbol{T}_j = -8\pi\mu[A_{j11}\,\boldsymbol{i} + B_{j11}\boldsymbol{j} + A_{j01}\,\boldsymbol{k}], \tag{2.20b}$$

where the six constant coefficients for each of the J spheres are known from the solution of (2.18).

We next consider the mobility problem in which the force and torque acting on each particle is prescribed and we seek to determine the resulting translational and angular velocities. To illustrate this, we examine the special case of a finite cluster of spheres falling freely under gravity in an unbounded medium. The balance between bouyancy and Stokes drag gives

$$-4\pi[E_{j11}\,\boldsymbol{i} + F_{j11}\boldsymbol{j} + E_{j01}\,\boldsymbol{k}] = -\tfrac{4}{3}\pi a_j^3(\rho_{s_j} - \rho)\,g\boldsymbol{k}, \tag{2.21a}$$

where ρ_{s_j} is the density of the jth sphere and ρ is the fluid density. The condition of zero torque gives

$$-8\pi\mu[A_{j11}\,\boldsymbol{i} + B_{j11}\boldsymbol{j} + A_{j01}\,\boldsymbol{k}] = 0. \tag{2.21b}$$

From (2.21) we evaluate the $6J$ constants as

$$A_{j01} = A_{j11} = B_{j11} = E_{j11} = F_{j11} = 0, \quad E_{j01} = \frac{a_j^3}{3}(\rho_{s_j} - \rho)\, g. \tag{2.22}$$

The $6J$ unknown particle translational and angular velocity components contained in (2.18) are exactly equal in number to the $6J$ constants evaluated in (2.22). Therefore the total number of equations and unknowns remain the same. The $6J$ unknown velocity components and the remaining $3JN(2M-1)$ unknown coefficients can be computed using any standard linear matrix reduction technique. After the unknown A_{jmn}–F_{jmn} coefficients have been determined from the solution of (2.18) they may be substituted into (2.11) to yield a relatively simple expression for the local fluid velocity at any point in the flow field. The more general problem involving a combination of a prescribed force and torque on some of the particles, and prescribed translation and angular velocities on the remaining particles may also be treated in a similar fashion.

Two special cases of the general three-dimensional theory described above will now be considered: the planar case and the axisymmetric case. For the planar case (the centres of all the spheres lie in the plane $Y = 0$) the constants A_{jmn}, D_{jmn} and F_{jmn} are all zero and so the number of unknowns is reduced to $3JMN - JN$. Moreover equations (2.18*c*, *e*, *h*, *j*–*l*, *n*) are identically zero because the velocity components V_k, $(\Omega_x)_k$ and $(\Omega_z)_k$ vanish and the integrands in these equations are odd functions about $\phi_k = \pi$. Thus for $m' = 0$, (2.18*a*, *f*) provide $2JN$ equations, for $m' = 1$, (2.18*b*, *g*, *m*) provide $3JN$ equations and for $m' = 2, 3, \ldots, M-1$, 2.18*d*, *i*, *o*) provide an additional $3JN(M-2)$ equations giving a total of $3JMN - JN$ equations, which is equal to the number of unknown constants. For these planar symmetric configurations, computation time can further be reduced by a factor of two by realizing that the remaining integrands are even functions about $\phi_k = \pi$ and performing the numerical integration only in the range $0 \leqslant \phi_k \leqslant \pi$. The axisymmetric case (the centres of all spheres lie along the Z-axis) can be deduced from the planar case. For axisymmetric configurations only the first term corresponding to $m = 0$ is needed in the infinite series. Therefore from (B 2), (B 8), and (B 14) the B_{j0n} coefficients are all zero and the number of unknowns is reduced to $2JN$. With $m' = 0$, equations (2.18*a*, *f*) provide $2JN$ equations for the unknown constants. It is worth noting that for the axisymmetric case the integrands of (2.18*a*, *f*) are independent of ϕ_k and the integration in ϕ_k can thus be performed analytically. The axisymmetric problem reduces to that solved by Gluckman *et al.* (1971) and therefore the accuracy of the method described herein is comparable with that of Gluckman *et al.* (1971) for the axisymmetric case.

To illustrate the application of the general three-dimensional theory to a specific problem, we consider the case of two identical spheres at arbitrary orientation settling freely under gravity as shown in figure 2. The boundary conditions are satisfied on two rings on the surface of each sphere and the Fourier series is truncated after the first two terms ($m = 0$ and 1). When specifying the rings on the surface of each sphere where conditions (2.15) are to be exactly satisfied, it is necessary to choose a pattern that is symmetric about the equatorial plane $\theta_k = \frac{1}{2}\pi$. Therefore the boundary condition is satisfied on two rings at angles θ_k and $\pi - \theta_k$ on each sphere and the boundary-collocation series includes terms for $m = 0$ and 1. The total number of equations obtained according to the expression $3JN(2M-1)$ (where J is the number of spheres; N is the number of rings and M is the order of truncation of the Fourier series) is 36. Therefore the unknown constants and velocity components

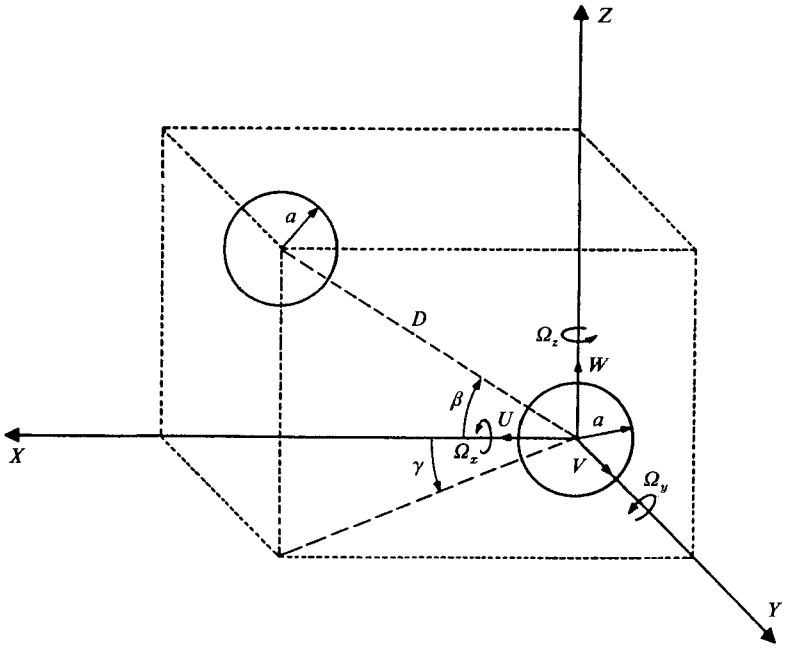

FIGURE 2. Two spheres settling freely under gravity at an arbitrary orientation.

to be obtained are: C_{j01}; A_{j02}; C_{j02}; F_{j02}; C_{j11}; D_{j11}; A_{j12}; B_{j12}; C_{j12}; D_{j12}; E_{j12}; F_{j12}; U_j; V_j; W_j; $(\Omega_x)_j$; $(\Omega_y)_j$; $(\Omega_x)_j$ for $j = 1, 2$.

From (2.18) we obtain 36 equations, or 18 equations for each sphere, or nine equations for each ring on each sphere. These nine equations are obtained for $m' = 0$ and $m' = 1$. For $m' = 0$ we obtain three equations from (18a, f, k) and for $m' = 1$ we obtain six equations from (2.18b, c, g, h, l, m). We get a corresponding set of nine equations for the other ring on the same sphere and two rings on the other sphere. The total set of 36 simultaneous equations forms the collocation matrix (Appendix D) and is solved numerically by a standard matrix reduction technique to obtain the values of unknown constants and the six velocity components.

3. Two-sphere solutions

In this section the accuracy and convergence of the basic collocation technique described in the previous section will be carefully examined by comparing the present results with the exact two-sphere solutions of Stimson & Jeffrey (1926) and Goldman *et al.* (1966), the axisymmetric multiparticle boundary collocation solutions of Gluckman *et al.* (1971) and the approximate planar collocation solutions of Ganatos *et al.* (1978).

Numerous test results were done to determine the best possible arrangement of the boundary collocation rings on the surface of each sphere for faster convergence of the collocation series. The single most important ring is at $\theta_k = \frac{1}{2}\pi$ (i.e. the equatorial plane of the sphere) since this ring covers the largest area on the surface of the sphere and also controls the projected area of the sphere. However, it was found that a singular matrix resulted if a boundary collocation ring was placed at $\theta_k = \frac{1}{2}\pi$. Therefore a pair of rings were placed at $\theta = \frac{1}{2}\pi \pm \alpha$ to overcome this problem, as was done by Gluckman *et al.* (1971) for axisymmetric flow. After doing several runs with

	Distance between sphere centres in sphere diameters, $D/2a$					
N	1.00245	1.04534	1.12763	1.54308	2.35241	6.13229
2	1.51104	1.50066	1.48161	1.39993	1.29180	1.12081
4	1.55182	1.53936	1.51672	1.42304	1.30230	1.12160
6	1.55002	1.53818	1.51639	1.42358	1.30245	1.12160
8	1.55005	1.53763	1.51605	1.42359	1.30246	—
10	1.55000	1.53757	1.15199	1.42358	1.30246	—
12	1.54935	1.53758	1.51599	1.42358	—	—
14	1.54936	1.53759	—	—	—	—
16	1.54937	1.53759	—	—	—	—
18	1.54937	—	—	—	—	—
Exact	1.54937	1.53759	1.51599	1.42358	1.30246	1.12160

TABLE 1. Velocity of two spheres settling axisymmetrically under gravity at different spacings. N is the number of boundary collocation rings on each sphere.

decreasing values of α it was determined that with $\alpha = 0.01°$ convergence to five digits was obtained. Additional pairs of boundary collocation rings were placed symmetrically about the equatorial plane in the upper and lower hemisphere equally spaced in the region $\theta_k = 0$ to $\theta_k = (\frac{1}{2}\pi - \alpha)$ and $\theta_k = (\frac{1}{2}\pi + \alpha)$ to $\theta = \pi$.

Table 1 shows computed values for the velocity of two identical spheres falling axisymmetrically under gravity as a function of interparticle spacing, $D/2a$, and the number of boundary collocation rings used on each sphere, N. The velocities have been non-dimensionalized by the terminal settling velocity of an isolated sphere. For this axisymmetric flow, only the first term in the Fourier series ($M = 1$) is used. Comparison with the exact results of Stimson & Jeffrey (1926) show that convergence to six significant figures can be obtained at all spacings. The rate of convergence is slowest at close spacings but increases rapidly with increasing spacing. This behaviour is consistent with the axisymmetric boundary collocation results of Gluckman *et al.* (1971). It should be noted that the method of Gluckman *et al.* (1971) of satisfying the no-slip boundary conditions at discrete points on the surface of each particle is equivalent to the present method since Gluckman *et al.*'s solutions actually satisfy the boundary conditions on rings owing to the axisymmetric symmetry of the problem. Gluckman *et al.* (1971) reported values for the drag coefficient factor for uniform flow past an axisymmetric chain of rigidly held spheres. Two equal spheres falling under gravity parallel to their line of centres fall with the same velocity and do not rotate. Therefore for this special case the reciprocal of the drag correction factor reported by Gluckman *et al.* (1971) is equal to the terminal settling velocity of two spheres at a given spacing. For the special axisymmetric case the method reduces to that of Gluckman *et al.* (1971) and the collocation series is identical term by term. Therefore comparison of table 1 with the solutions of Gluckman *et al.* (1971) shows the rate of convergence of the two methods to be identical and the accuracy of this method is comparable with that of Gluckman *et al.* (1971) for the axisymmetric case. However, for a given number of boundary collocation rings used on each sphere N, before convergence is achieved, the two sets of results are not exactly identical

N	M	U	V	W	Ω_x	Ω_y	Ω_z
				(*a*) $\gamma = 0, \beta = 0°$			
2	2	0		−1.1628		0.03444	
2	3	0		−1.1627		0.03443	
2	4	0		−1.1627		0.03443	
4	2	0		−1.1642		0.03381	
4	3	0		−1.1642		0.03381	
4	4	0		−1.1641		0.03381	
4	5	0		−1.1641		0.03381	
6	2	0		−1.1642		0.03383	
6	3	0		−1.1641		0.03383	
6	4	0		−1.1641		0.03383	
Exact solution		0		−1.1641		0.03383	
				(*b*) $\gamma = 0, \beta = 30°$			
2	2	−0.06165		−1.2024		0.02897	
2	3	−0.06063		−1.2017		0.02912	
2	4	−0.06059		−1.2017		0.02913	
2	5	−0.06059		−1.2017		0.02913	
4	2	−0.06115		−1.1994		0.02914	
4	3	−0.06001		−1.1987		0.02930	
4	4	−0.05995		−1.1987		0.02931	
4	5	−0.05995		−1.1987		0.02931	
6	2	−0.06110		−1.1994		0.02913	
6	3	−0.05996		−1.1987		0.02930	
6	4	−0.05991		−1.1987		0.02930	
6	5	−0.05991		−1.1987		0.02930	
Exact solution		−0.05991		−1.1987		0.02930	
				(*c*) $\gamma = 0, \beta = 60°$			
2	2	−0.04988		−1.2656		0.01602	
2	3	−0.04977		−1.2655		0.01611	
2	4	−0.04977		−1.2655		0.01611	
4	2	−0.05997		−1.2682		0.01679	
4	3	−0.05982		−1.2679		0.01691	
4	4	−0.05982		−1.2679		0.01691	
6	2	−0.06006		−1.2681		0.01679	
6	3	−0.05991		−1.2679		0.01691	
6	4	−0.05991		−1.2679		0.01691	
6	5	−0.05991		−1.2679		0.01691	
Exact solution		−0.05991		−1.2679		0.01691	
				(*d*) $\gamma = 0, \beta = 90°$			
2	1	0		−1.2918		0	
4	1	0		−1.3023		0	
6	1	0		−1.3025		0	
Exact solution		0		−1.3025		0	
				(*e*) $\gamma = 30, \beta = 0°$			
2	2	0	0	−1.1628	0.01722	0.02982	0
2	3	0	0	−1.1627	0.01722	0.02982	0
2	4	0	0	−1.1627	0.01722	0.02982	0
4	2	0	0	−1.1642	0.01690	0.02928	0
4	3	0	0	−1.1642	0.01690	0.02928	0
4	4	0	0	−1.1642	0.01690	0.02928	0
6	2	0	0	−1.1642	0.01692	0.02930	0
6	3	0	0	−1.1641	0.01691	0.02930	0
6	4	0	0	−1.1641	0.01691	0.02930	0
Exact solution		0	0	−1.1641	0.01691	0.02930	0

Table 2 (*cont.*)

N	M	U	V	W	Ω_x	Ω_y	Ω_z
			(*f*) $\gamma = 30, \beta = 30°$				
2	2	−0.05339	−0.03083	−1.2024	0.01449	0.02509	0
2	3	−0.05251	−0.03031	−1.2017	0.01456	0.02522	0
2	4	−0.05247	−0.03030	−1.2017	0.01456	0.02523	0
2	5	−0.05247	−0.03030	−1.2017	0.01456	0.02523	0
4	2	−0.05296	−0.03058	−1.1994	0.01457	0.02524	0
4	3	−0.05197	−0.03001	−1.1987	0.01465	0.02538	0
4	4	−0.05192	−0.02998	−1.1987	0.01466	0.02539	0
4	5	−0.05192	−0.02998	−1.1987	0.01466	0.02539	0
6	2	−0.05292	−0.03055	−1.1994	0.01456	0.02522	0
6	3	−0.05193	−0.02998	−1.1987	0.01464	0.02536	0
6	4	−0.05188	−0.02995	−1.1987	0.01465	0.02537	0
Exact solution		−0.05188	−0.02995	−1.1987	0.01465	0.02537	0
			(*g*) $\gamma = 30, \beta = 60°$				
2	2	−0.04300	−0.02494	−1.2656	0.00801	0.01388	0
2	3	−0.04310	−0.02489	−1.2655	0.00805	0.01395	0
2	4	−0.04310	−0.02489	−1.2655	0.00805	0.01395	0
4	2	−0.05193	−0.02998	−1.2682	0.00839	0.01454	0
4	3	−0.05180	−0.02991	−1.2679	0.00845	0.01464	0
4	4	−0.05180	−0.02991	−1.2679	0.00845	0.01464	0
6	2	−0.05201	−0.03003	−1.2681	0.00840	0.01454	0
6	3	−0.05188	−0.02996	−1.2679	0.00841	0.01465	0
6	4	−0.05188	−0.02995	−1.2679	0.00846	0.01465	0
Exact solution		−0.05188	−0.02995	−1.2679	0.00846	0.01465	0
			(*h*) $\gamma = 60, \beta = 0°$				
2	2	0	0	−1.1628	0.02982	0.01726	0
2	3	0	0	−1.1628	0.02982	0.01727	0
2	4	0	0	−1.1627	0.02982	0.01722	0
2	5	0	0	−1.1627	0.02982	0.01722	0
4	2	0	0	−1.1642	0.02928	0.01690	0
4	3	0	0	−1.1642	0.02928	0.01690	0
4	4	0	0	−1.1641	0.02928	0.01690	0
6	2	0	0	−1.1642	0.02930	0.01692	0
6	3	0	0	−1.1641	0.02930	0.01691	0
6	4	0	0	−1.1641	0.02930	0.01691	0
Exact solution		0	0	−1.1641	0.02930	0.01691	0
			(*i*) $\gamma = 60, \beta = 30°$				
2	2	−0.03083	−0.05339	−1.2024	0.02509	0.01449	0
2	3	−0.03032	−0.05251	−1.2017	0.02522	0.01456	0
2	4	−0.03030	−0.05247	−1.2017	0.02525	0.01456	0
2	5	−0.03030	−0.05247	−1.2017	0.02523	0.01456	0
4	2	−0.03058	−0.05296	−1.1994	0.02524	0.01457	0
4	3	−0.03000	−0.05197	−1.1987	0.02537	0.01465	0
4	4	−0.02998	−0.05192	−1.1987	0.02539	0.01466	0
4	5	−0.02998	−0.05192	−1.1987	0.02539	0.01466	0
6	2	−0.03055	−0.05292	−1.1994	0.02522	0.01456	0
6	3	−0.02998	−0.05193	−1.1987	0.02536	0.01464	0
6	4	−0.02995	−0.01588	−1.1987	0.02537	0.01465	0
6	5	−0.02995	−0.05188	−1.1987	0.02537	0.01465	0
Exact solution		−0.02995	−0.05188	−1.1987	0.02537	0.01465	0

N	M	U	V	W	Ω_x	Ω_y	Ω_z
			(*j*) $\gamma = 60, \beta = 60°$				
2	2	−0.02494	−0.04320	−1.2656	0.01388	0.00801	0
2	3	−0.02489	−0.04310	−1.2655	0.01395	0.00805	0
2	4	−0.02489	−0.04310	−1.2655	0.01395	0.00805	0
4	2	−0.02998	−0.05193	−1.2682	0.01454	0.00839	0
4	3	−0.02991	−0.05180	−1.2679	0.01464	0.00845	0
4	4	−0.02991	−0.05180	−1.2679	0.01464	0.00845	0
6	2	−0.03003	−0.05201	−1.2681	0.01454	0.00840	0
6	3	−0.02996	−0.05188	−1.2679	0.01465	0.00846	0
6	4	−0.02995	−0.05188	−1.2679	0.01465	0.00846	0
Exact solution		−0.02995	−0.05188	−1.2679	0.01465	0.00846	0
			(*k*) $\gamma = 90, \beta = 0°$				
2	2		0	−1.1628	0.03444		
2	3		0	−1.1628	0.03443		
2	4		0	−1.1627	0.03443		
4	2		0	−1.1642	0.03381		
4	3		0	−1.1642	0.03381		
4	4		0	−1.1641	0.03381		
6	2		0	−1.1642	0.03383		
6	3		0	−1.1641	0.03383		
6	4		0	−1.1641	0.03383		
Exact solution			0	−1.1641	0.03383		
			(*l*) $\gamma = 90, \beta = 30°$				
2	2		−0.06164	−1.2024	0.02897		
2	3		−0.06101	−1.2020	0.02906		
2	4		−0.06059	−1.2017	0.02913		
2	5		−0.06059	−1.2017	0.02913		
4	2		−0.06115	−1.1994	0.02914		
4	3		−0.06001	−1.1987	0.02930		
4	4		−0.05995	−1.1987	0.02931		
4	5		−0.05995	−1.1987	0.02931		
6	2		−0.06110	−1.1994	0.02913		
6	3		−0.05996	−1.1987	0.02930		
6	4		−0.05991	−1.1987	0.02930		
6	5		−0.05991	−1.1987	0.02930		
Exact solution			−0.05991	−1.1987	0.02930		
			(*m*) $\gamma = 90, \beta = 60°$				
2	2		−0.04990	−1.2656	0.01602		
2	3		−0.04977	−1.2655	0.01611		
2	4		−0.04977	−1.2655	0.01611		
4	2		−0.05997	−1.2682	0.01679		
4	3		−0.05982	−1.2679	0.01691		
4	4		−0.05982	−1.2679	0.01691		
6	2		−0.06006	−1.2681	0.01679		
6	3		−0.05991	−1.2679	0.01691		
6	4		−0.05991	−1.2679	0.01691		
Exact solution			−0.05991	−1.2679	0.01691		

TABLE 2(*a–m*). Velocities of two spheres settling freely under gravity at an arbitrary orientation of various values of γ and β. $D/2a = 2.3524096$; N is the number of rings on each sphere; M is the number of eigenfunctions retained in the azimuthal direction; U, V, W, Ω_x, Ω_y and Ω_z are the translational and rotational velocity components.

because the collocation rings are not placed exactly at the same values of θ_k as the collocation points in Gluckman *et al.*'s paper.

Table 2 (*a–m*) shows the computed translational and rotational Cartesian velocity components for two spheres settling freely under gravity in 13 different combinations of elevation angle β and azimuthal orientation angle γ at a spacing of 2.3524096 diameters (see figure 2). All the results for the various orientations converge to the exact solution of Goldman *et al.* (1966) to five decimal places with increasing values of M and N. Moreover, it is interesting to note the pattern of convergence. For non-axisymmetric configurations we need at least two terms in the series (corresponding to $m = 0$ and $m = 1$) to introduce dependence of the solution on the azimuthal angle ϕ_k. At this spacing six rings and up to 4 terms of the Fourier series are needed to produce five-digit accuracy in the translational and angular velocity components. The number of rings and the order of truncation of the Fourier series M required for a given accuracy are nearly independent of the elevation angle β and azimuthal orientation angle γ except in the limit as the axisymmeric case is approached ($\beta \rightarrow 90°$) where only the first term in the Fourier series is required ($M = 1$).

Table 3 shows convergence results for the severe case of two spheres settling freely under gravity in a vertical plane at an elevation angle $\beta = 60°$ (see figure 2) and a spacing of 1.1276260 diameters between centres. It is seen that all three velocity components converge to the exact solutions of Goldman *et al.* (1966) to five decimal places with increasing N and M even at this close spacing. This accuracy is achieved with $N = 10$ and $M = 7$. In contrast, for this configuration the approximate collocation solutions of Ganatos *et al.* (1978) gave an error of 3%, 8% and 12% in W, U and Ω_y respectively.

Examination of tables 1, 2 and 3 shows that the number of rings required on each particle to achieve a given accuracy of the result depends only on the interparticle spacing and is independent of the relative orientation of the two particles. As a rule of thumb one could use table 1 to estimate the number of rings N required for a given accuracy at any orientation. The minimum order of truncation of the Fourier series M for the same accuracy is roughly 70% of the required number of rings N at that spacing, except for nearly axisymmetric configurations where a smaller value of M could be used.

Table 4 presents the forces and torques exerted by two unequal spheres ($a_1/a_2 = 2$) with interparticle gap width equal to the smaller radius ($S/a_2 = 1$) moving perpendicular to the line joining their centres with equal velocities. These results reproduce the exact solutions of Davis (1969). These results again demonstrate the convergence to the exact values with increasing values of M and N. In this study we have used the same value of M and N for both the small and the large sphere. The rate of convergence for unequal spheres can be greatly improved by placing a greater number of rings on the larger sphere depending on the size ratio, as was done by Liao & Krueger (1980) for the axisymmetric motion of two unequal spheroids.

The two-sphere results presented in this section show that when the order of truncation of the Fourier series is increased for a fixed number of boundary rings, the solution converges to a particular value, and when the number of boundary rings is increased, the solution converges to the exact value. So, depending upon the level of accuracy needed the number of boundary rings and the order of truncation can be fixed accordingly. It is seen here that convergence with increasing values of M and N is very rapid and systematic and the convergence problems encountered by Ganatos *et al.* (1978) for the settling of two spheres at an arbitrary orientation are

N	M	U	W	Ω_y
2	2	−0.03166	−1.4663	0.05544
2	3	−0.03046	−1.4661	0.05667
2	4	−0.03035	−1.4662	0.05669
2	5	−0.03034	−1.4662	0.05669
2	6	−0.03034	−1.4662	0.05669
4	2	−0.06595	−1.4778	0.06293
4	3	−0.06522	−1.4778	0.06566
4	4	−0.06520	−1.4777	0.06570
4	5	−0.06520	−1.4777	0.06569
4	6	−0.06520	−1.4777	0.06569
6	2	−0.06617	−1.4794	0.06282
6	3	−0.06540	−1.4782	0.06616
6	4	−0.06538	−1.4781	0.06624
6	5	−0.06538	−1.4781	0.06625
6	6	−0.06538	−1.4781	0.06623
6	7	−0.06538	−1.4781	0.06623
8	2	−0.06635	−1.4795	0.06238
8	3	−0.06543	−1.4783	0.06585
8	4	−0.06542	−1.4782	0.06583
8	5	−0.06542	−1.4782	0.06575
8	6	−0.06542	−1.4782	0.06574
8	7	−0.06542	−1.4782	0.06574
10	2	−0.06640	−1.4795	0.06236
10	3	−0.06547	−1.4783	0.06578
10	4	−0.06547	−1.4782	0.06580
10	5	−0.06547	−1.4782	0.06572
10	6	−0.06547	−1.4782	0.06570
10	7	−0.06547	−1.4782	0.06571
Exact solution		−0.06547	−1.4782	0.06571

TABLE 3. Velocities of two spheres settling freely under gravity at an arbitrary orientation of $\gamma = 0.0°$, $\beta = 60.0°$. $D/2a = 1.127626$; N is the number of rings on each sphere; M is the number of eigenfunctions retained in the azimuthal direction; U, V, W, Ω_x, Ω_y and Ω_z are the translational and rotational velocity components.

completely eliminated by satisfying the no-slip boundary conditions on entire rings on the surface of each sphere instead of discrete boundary points.

We next consider the accuracy of the method in predicting the local fluid velocity field. Figure 3(*a*) shows the flow field for uniform flow past two spheres whose line of centres lies parallel to the direction of flow at a centre-to-centre distance of 1.5430805 particle diameters. Figure 3(*b*), which is an enlargement of the flow field in the gap between the two spheres, shows that a separated region of closed circulation develops between the two spheres exactly as predicted by the exact theory of Davis *et al.* (1976). In preparing figure 3 we used six collocation rings on each sphere and retained four terms in the Fourier series.

Thus we see that the present method of solution not only can predict global quantities such as the force and torque on each particle but can accurately predict the fine structure of the local fluid velocity fields as well. It is worth noting that figure 3, and all other figures in this paper showing solutions for the fluid velocity field, were prepared by transferring the mainframe digital data to an IBM PC AT and then plotting the data as shown in these figures with an HP 7440A plotter using the graphics capabilities of the AUTOCAD software.

N	M	F_1	T_1	F_2	T_2
2	2	0.8754	0.0649	0.6540	−0.0817
2	3	0.8750	0.0655	0.6595	−0.0816
2	4	0.8748	0.0658	0.6612	−0.0816
2	5	0.8747	0.0659	0.6617	−0.0816
2	6	0.8747	0.0660	0.6618	−0.0816
4	2	0.8691	0.0580	0.6561	−0.0787
4	3	0.8684	0.0584	0.6602	−0.0787
4	4	0.8681	0.0585	0.6613	−0.0783
4	5	0.8680	0.0586	0.6615	−0.0783
4	6	0.8680	0.0586	0.6616	−0.0783
6	2	0.8697	0.0589	0.6561	−0.0786
6	3	0.8691	0.0594	0.6602	−0.0782
6	4	0.8689	0.0596	0.6612	−0.0781
6	5	0.8688	0.0596	0.6615	−0.0781
6	6	0.8688	0.0596	0.6616	−0.0781
8	2	0.8696	0.0589	0.6561	−0.0786
8	3	0.8690	0.0593	0.6602	−0.0782
8	4	0.8687	0.0595	0.6613	−0.0781
8	5	0.8686	0.0596	0.6616	−0.0781
8	6	0.8686	0.0596	0.6616	−0.0781
Exact solutions of Davis (1969)		0.8686	0.0596	0.6616	−0.0781

TABLE 4. Force and torque on two unequal spheres. $a_1/a_2 = 2.0$, $S/a_2 = 1.0$, N is the number of collocation rings on each sphere. M is the order of truncation of Fourier series.

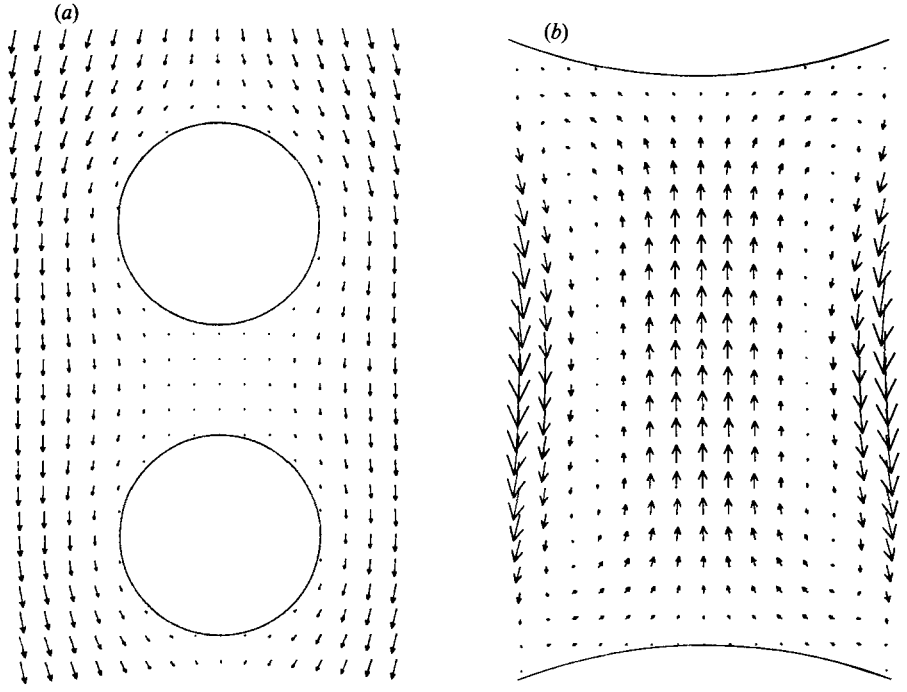

FIGURE 3. (*a*) Fluid velocity field for flow past two axisymmetrically oriented spheres, $D/2a = 1.543$. (*b*) Enlarged view of the fluid velocity field in the gap.

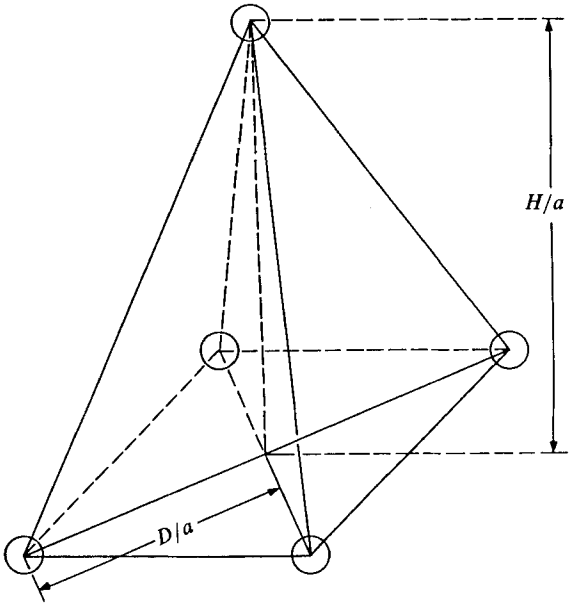

FIGURE 4. Multiparticle configuration of five spheres.

4. Arbitrary multisphere configurations

In this section we present results for some interesting configurations involving a finite cluster of spherical particles.

Consider J identical spheres settling under gravity arranged such that at the instant of time under consideration $(J-1)$ spheres lie at the vertices of a regular horizontal polygon of radius D (measured in sphere radii) and the Jth sphere is located at the centre of the regular polygon at a vertical distance H (in sphere radii) above the horizontal plane of the polygon as shown in figure 4. If the jth sphere lies in the same horizontal plane of the polygon, it falls faster than the spheres at the vertices of the regular horizontal polygon, but if it lies in a plane above that of the polygon, and if H is sufficiently large, the spheres at the vertices of the horizontal polygon fall faster, leaving the Jth sphere behind. Thus there is a critical spacing H for a particular value of D at which instant the whole configuration of spheres fall at the same speed. Figure 5 shows a plot for the critical spacing ratio H/D as a function of the polygon radius D for 3-, 4-, 5- and 6-sphere configurations. As the ratio D/a is increased the critical spacing H/D increases and asymptotes to a constant value as the spheres behave like point forces. As the number of spheres in the polygon is increased, the critical spacing ratio H/D monotonically decreases. The curve for $J = 3$, which represents a vertical planar configuration of particles, is in excellent agreement with the approximate planar collocation results of Ganatos *et al.* (1978).

Next we look at a steady configuration where a sphere is placed below as well as above the regular horizontal polygon as shown in figure 6. Figure 7 shows a plot for the ratio of critical spacing H/D as a function of the polygon radius D for 4-, 5- and 6-sphere configurations. It should be noted that although the configurations shown in figure 7 are steady, they are unstable. If any of the spheres in the cluster are

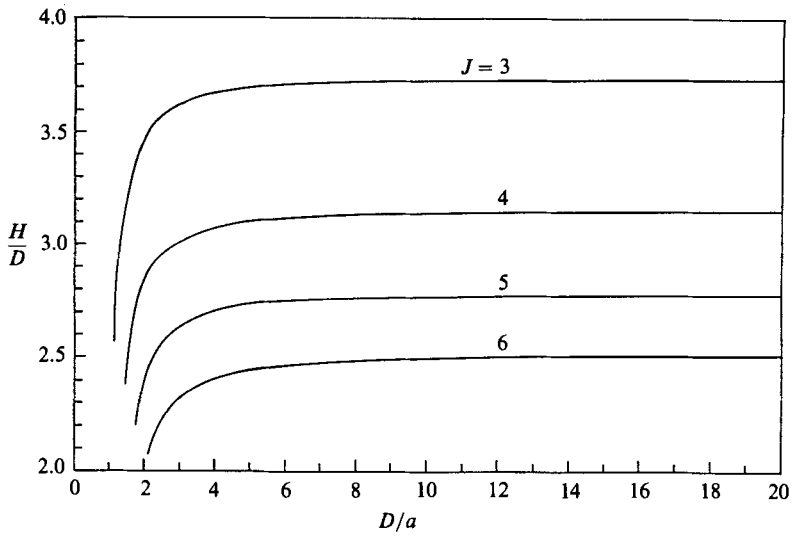

FIGURE 5. Plot of critical spacing for configurations of 3, 4, 5 and 6 spheres as shown in figure 4.

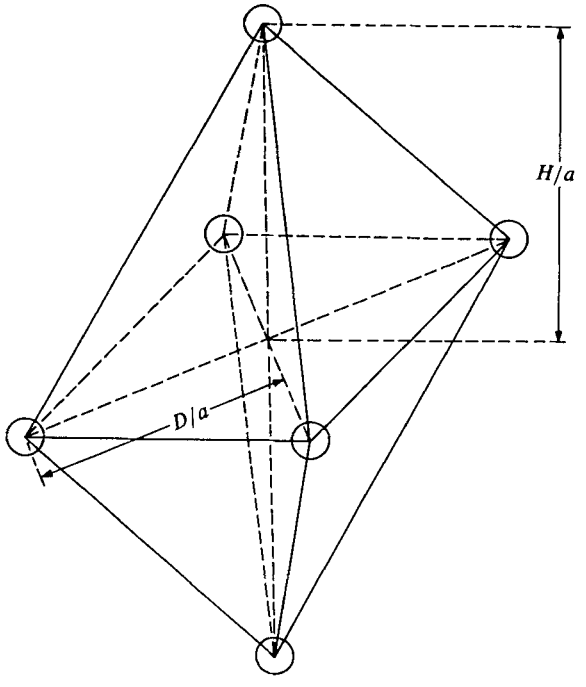

FIGURE 6. Steady configuration of six spheres.

slightly displaced from their critical position, the configuration will break up as it settles.

We now examine the behaviour of a sphere settling freely under gravity in the presence of other fixed spheres. In this example, $J-1$ spheres are fixed at the corners of a horizontal regular polygon and the Jth sphere is allowed to settle freely under

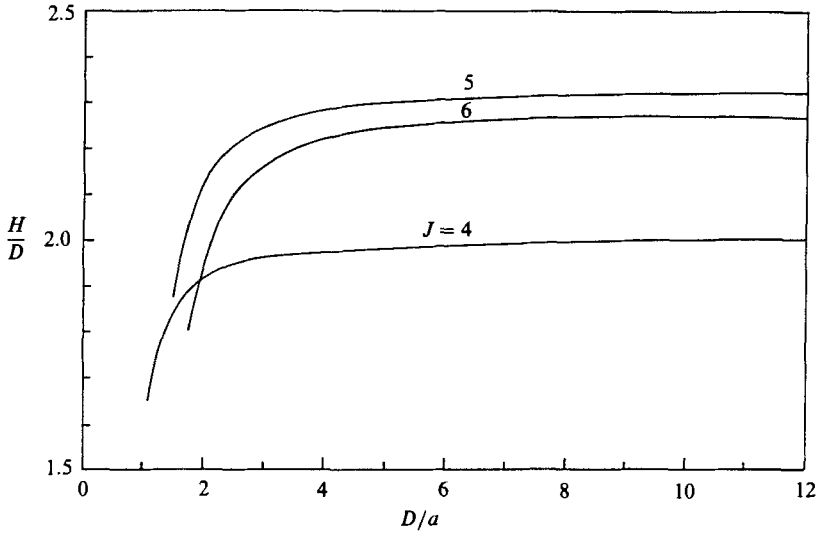

FIGURE 7. Plot of critical spacing for steady configurations of 4, 5 and 6 spheres as shown in figure 6.

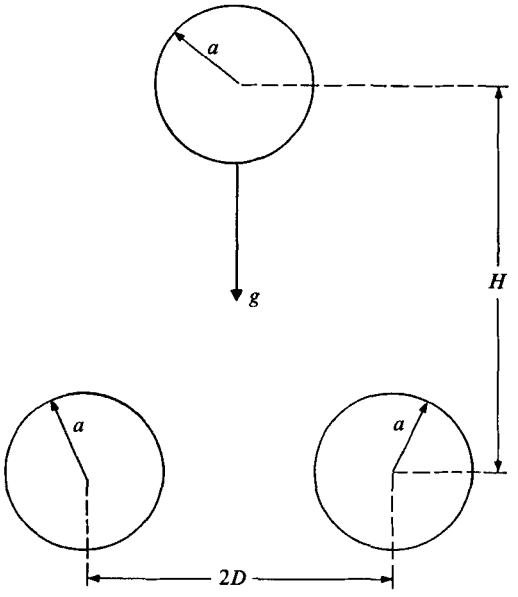

FIGURE 8. Schematic diagram of a sphere settling under gravity between two fixed spheres in a vertical plane.

gravity along a line perpendicular to the plane of the fixed spheres and passing through the centre of the polygon as shown in figures 8 and 9. The settling sphere will have a vertical velocity component but no lateral drift velocity owing to the symmetry of the flow. Therefore by calculating the velocity of the settling sphere as a function of vertical distance from the horizontal plane of the polygon it is possible to describe the complete time history of the falling motion.

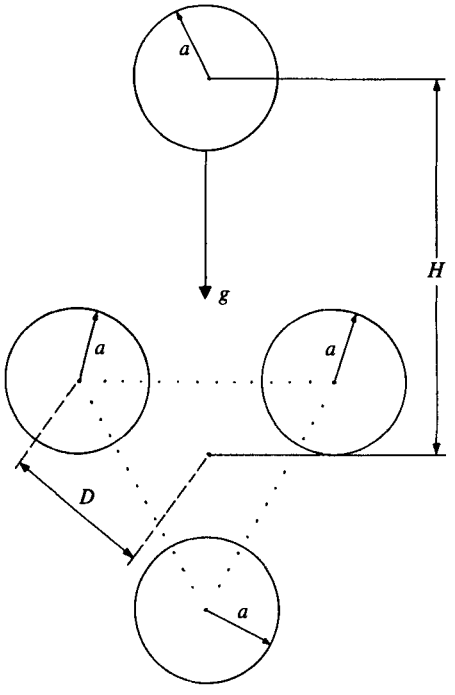

FIGURE 9. Schematic diagram of a sphere settling under gravity through three fixed spheres placed at the vertices of a horizontal equilateral triangle.

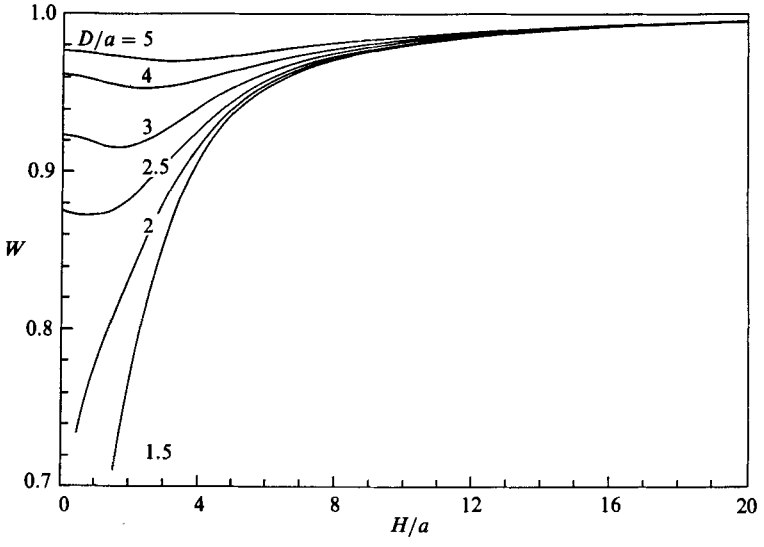

FIGURE 10. Settling velocity of a sphere W, non-dimensionalized by the settling velocity of an isolated sphere, falling between two fixed spheres as shown in figure 8.

Solutions are presented for two such cases. Figure 8 shows a 3-sphere configuration where a sphere is freely settling owing to gravity through two fixed spheres. Figure 9 shows a 4-sphere configuration where a sphere is falling through three fixed spheres placed at the vertices of a horizontal equilateral triangle. Figures 10 and 11 show plots of the ratio of the instantaneous settling velocity of the falling sphere to the

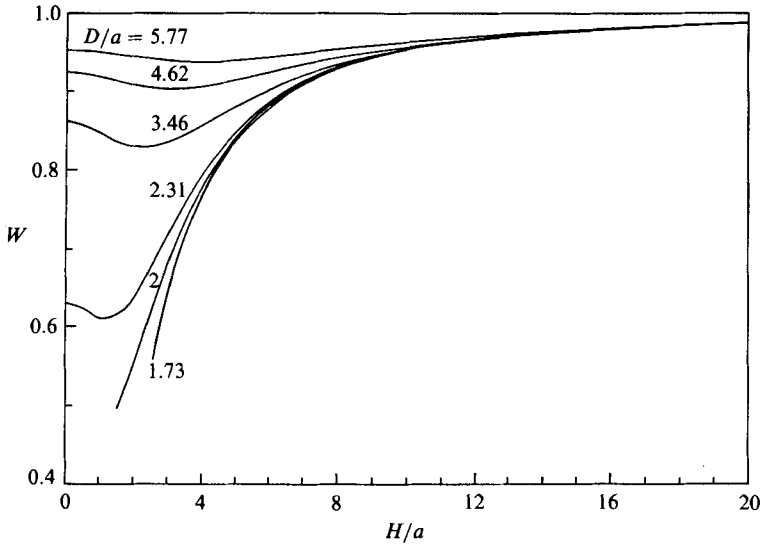

FIGURE 11. Settling velocity of a sphere W, non-dimensionalized by the settling velocity of an isolated sphere, falling between three fixed spheres as shown in figure 9.

settling velocity of an isolated sphere as a function of vertical distance H from the plane of the fixed spheres for various centre-to-centre distances of the fixed spheres. Interestingly, the settling velocity of the sphere is not at its smallest value when it is in the plane of the fixed spheres but has a minimum before it approaches the plane of the fixed spheres. For $D/a = 5$ the minimum velocity occurs at roughly $H/a = 3.5$ for two fixed spheres, and for $D/a = 5.8$ the minimum velocity occurs at $H/a = 4.5$ for three fixed spheres. As the ratio D/a is decreased, the minimum value occurs closer to the plane of the fixed spheres. The velocity of the falling sphere drops to zero when the centre-to-centre distance between the fixed spheres is such that the settling sphere just fits between the fixed spheres ($D/a = 2$ for three and four spheres). The reason why the settling sphere has a minimum velocity when it is above the plane of the fixed spheres is that it views a greater exposed area of the fixed spheres from this position than when it is in the same plane as the fixed spheres. This behaviour is consistent with the results of Dagan, Weinbaum & Pfeffer (1983) who considered the motion of a sphere through a circular hole in a planar wall.

We next consider the flow field of several interesting three-particle configurations. Figure 12 shows the fluid velocity field for uniform flow past three spheres arranged at the corners of an equilateral triangle with one base of the triangle parallel to the direction of flow. Comparison with figure 3 shows that the presence of the third sphere changes the velocity profile considerably. Owing to the presence of the sphere on the right, the fluid in the gap between the top and bottom spheres has only one closed loop of circulating fluid in the plane of symmetry. However if this whole configuration is rotated by 60° so that one base of the triangle is perpendicular to the direction of the fluid flow, as shown in figure 13, there is no longer a region of closed circulation of fluid between the spheres. It is also seen from these figures how well the present method is able to satisfy the no-slip boundary conditions on the surface of each sphere. In all these runs for a centre-to-centre spacing of 1.543 086 diameters we used six collocation rings on each sphere and retained four terms in the Fourier series.

The L-shaped configuration settling under gravity is another interesting case to

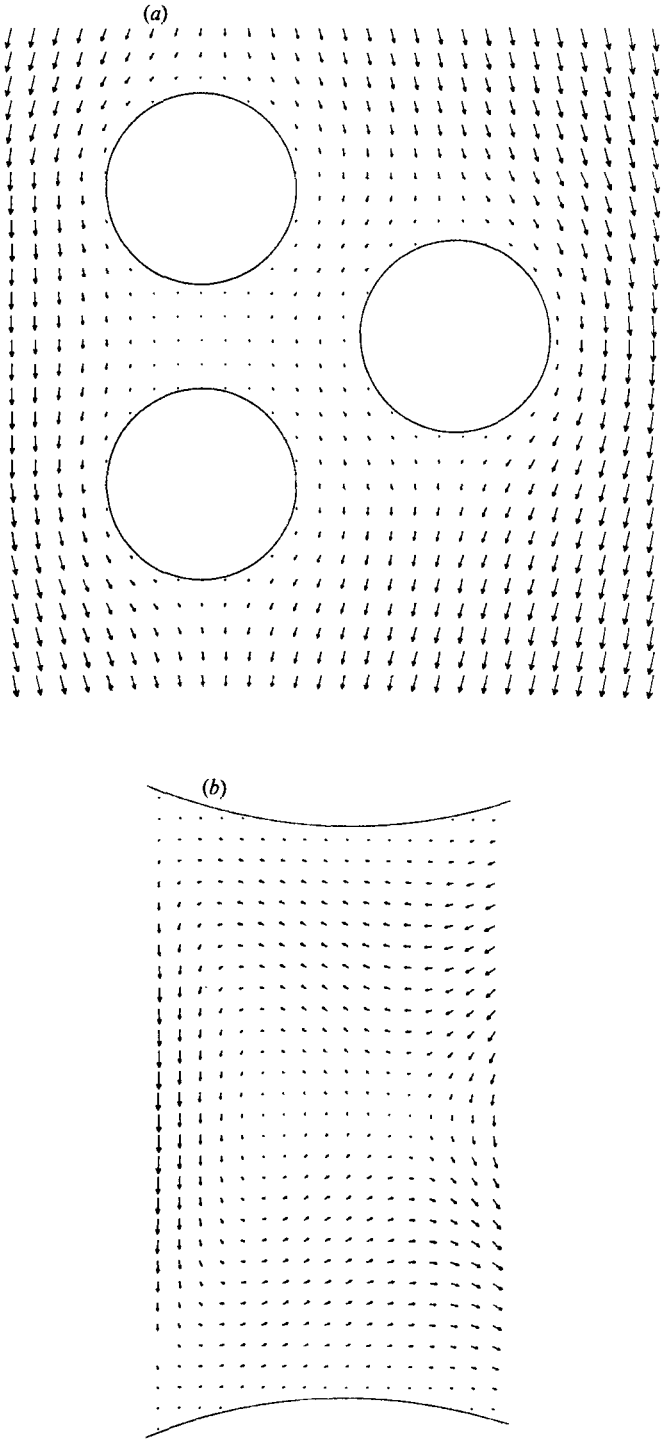

FIGURE 12. (*a*) Fluid velocity field for flow past three rigidly held spheres placed at the corners of an equilateral triangle. Base of triangle is oriented parallel to the direction of fluid flow. $D/2a = 1.543$. (*b*) Enlarged view of the flow field in the gap.

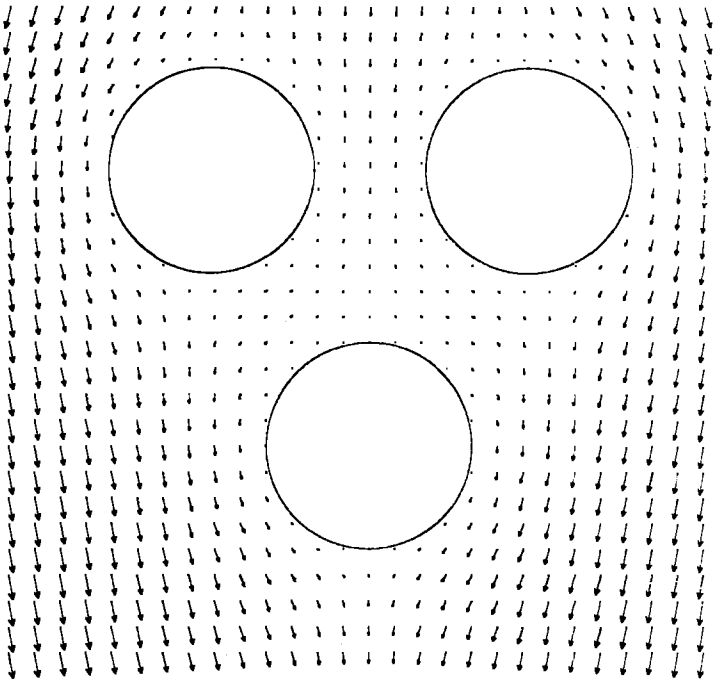

FIGURE 13. Fluid velocity field for flow past three rigidly held spheres placed at the corners of an equilateral triangle. Base of triangle is oriented perpendicular to the direction of flow. $D/2a = 1.543$.

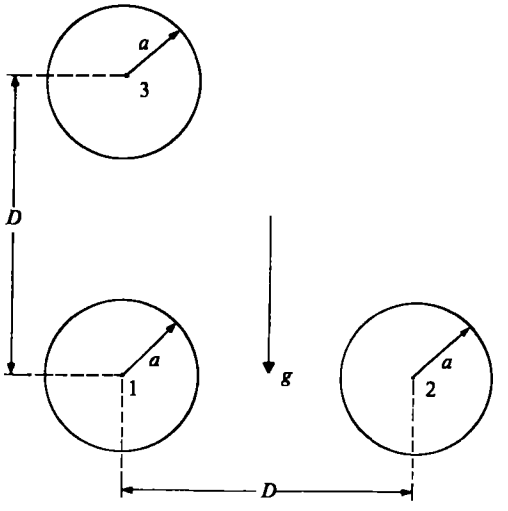

FIGURE 14. Three spheres in an L-shaped configuration settling freely under gravity.

look at. Here three spheres are placed at the corners of a right-angle triangle as shown in figure 14. According to the method of paired interactions sphere 1 placed at the vertex of the right angle (corner sphere) should have only a vertical velocity component and no lateral drift velocity. However using the exact theory, we find that it also has a horizontal component which arises from the interaction between spheres 2 and 3 on 1. The intriguing feature is that when the interparticle distance

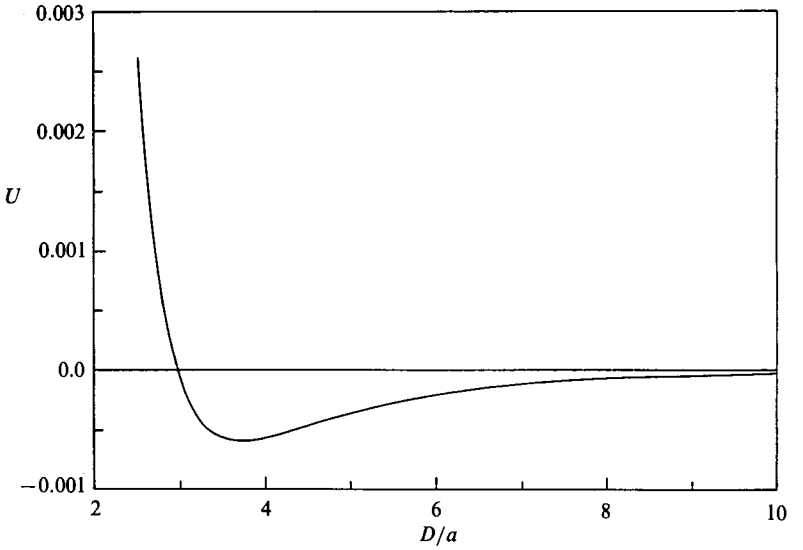

FIGURE 15. Plot of the lateral drift velocity U of the corner sphere (sphere 1) in the L-shaped configuration shown in figure 14. The velocity is non-dimensionalized by the settling velocity of an isolated sphere.

between the three spheres is increased the horizontal velocity component of the corner sphere decreases and at a spacing of approximately 1.48 diameters it changes sign before decaying to zero. Figure 15 shows a plot of the converged lateral drift velocity of the corner sphere with the interparticle distance using six boundary collocation rings on each sphere and five terms in the Fourier series. The reason for this peculiar behaviour can be deduced by considering the flow field as viewed in a reference frame that is translating with the corner sphere as shown in figures 16 and 17. The fluid velocity profile around the corner sphere is shown in figure 16 for an interparticle spacing of 1.75 diameters where the corner sphere moves to the left, and in figure 17 for an interparticle spacing of 1.3 diameters where the corner sphere moves to the right. When the three spheres are falling under gravity the amount of fluid entering the gap between spheres 1 and 2 is more than the fluid leaving the gap, owing to the inhibiting action of sphere 3. This effect causes an accumulation of fluid between spheres 1 and 2, tending to push them apart. When the interparticle distance is small (less than 1.48 diameters) the strong hydrodynamic interaction between spheres 2 and 3 causes the whole configuration to move to the right. However when the interparticle distance is greater than 1.48 diameters the hydrodynamic interaction weakens and the corner sphere moves to the left whereas spheres 1 and 2 move to the right. As the interparticle distance is further increased the hydrodynamic interaction further weakens and the lateral drift velocity of the corner sphere decays to zero.

Next we look at a straight chain of three unequal spheres fixed in a uniform flow. For equal-sized spheres the central sphere experiences the least drag. However, the size of the central sphere can be increased so that all three spheres in the straight chain will experience the same force. In figure 18(a, b) three spheres are arranged in a straight line which is either parallel or perpendicular to the direction of flow. The ratio of radii of the inner and outer sphere (a_1/a_2) is such that the drag force on all the three spheres in the chain is equal. Figure 19 shows a plot of the ratio of radii for

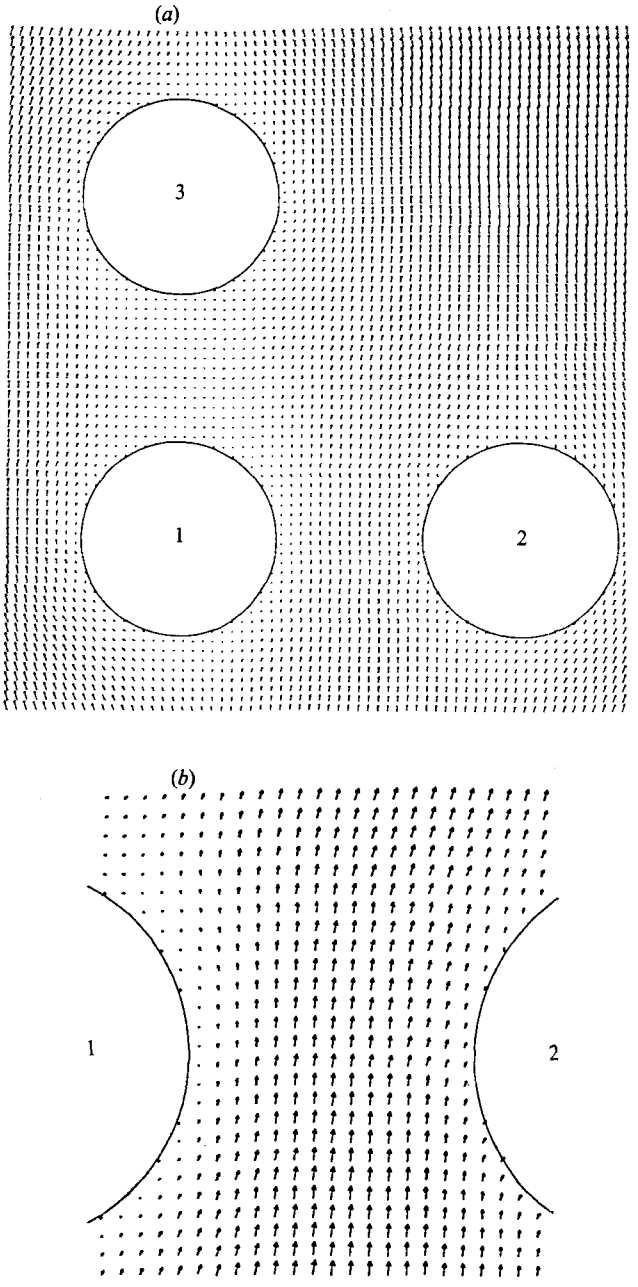

FIGURE 16. (*a*) Flow field in the velocity of three spheres arranged in an L-shaped configuration falling freely under gravity, $D/a = 3.5$. Fluid velocities are measured relative to the translational velocity of the centre of sphere 1. (*b*) Enlarged view of the flow field in the gap between spheres 1 and 2.

different interparticle spacings for both chains. It is observed that the variation in the ratio of radii is greater for increasing interparticle spacing when the chain is parallel to the direction of flow since the shielding effect of the outer spheres on the inner sphere is greater in this case. From these two plots we can obtain the ratio of radii for a particular interparticle spacing for any orientation of a straight chain of

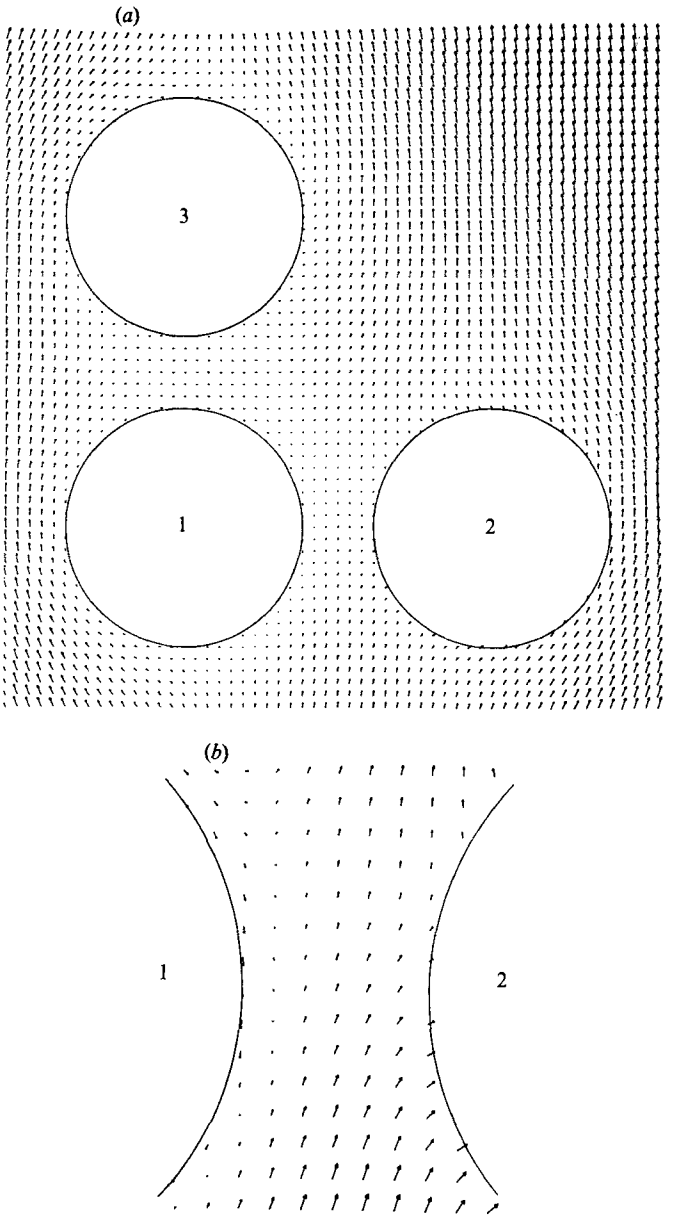

FIGURE 17. (*a*) Flow field in the vicinity of three spheres arranged in an L-shaped configuration falling freely under gravity, $D/a = 2.6$. Fluid velocities are measured relative to the translational velocity of the centre of sphere 1. (*b*) Enlarged view of the flow field in the gap between spheres 1 and 2.

three spheres with respect to the direction of flow having equal drag force on all the spheres using the formula

$$\left(\frac{a_1}{a_2}\right)_\beta = \left(\frac{a_1}{a_2}\right)_\perp \cos\beta + \left(\frac{a_1}{a_2}\right)_\parallel \sin\beta, \tag{4.1}$$

where β is any orientation angle measured from the horizontal axis, and $(a_1/a_2)_\perp$ and $(a_1/a_2)_\parallel$ are the ratio of radii for the same interparticle spacing when the chain is perpendicular and parallel to the direction of flow respectively.

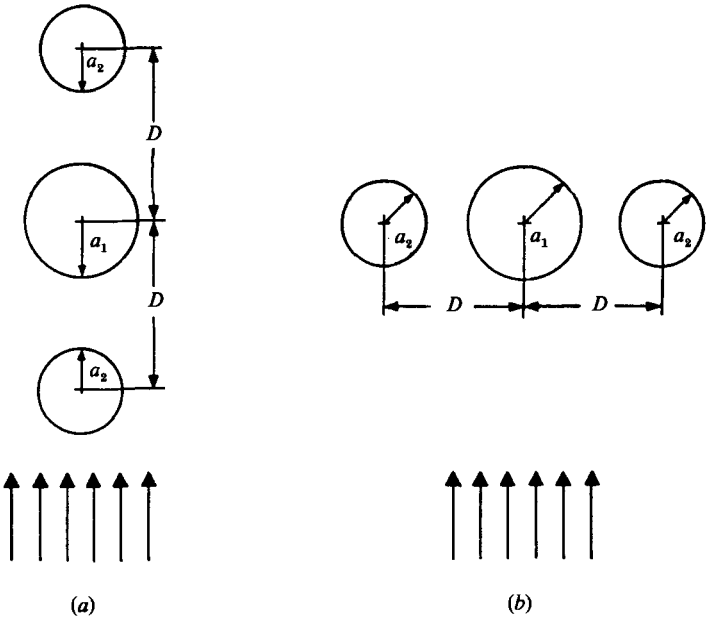

FIGURE 18. Schematic diagram of uniform flow past a straight chain of three rigidly held unequal spheres. The two outer spheres are identical and the central sphere is larger. Chain oriented (*a*) parallel and (*b*) perpendicular to the direction of flow.

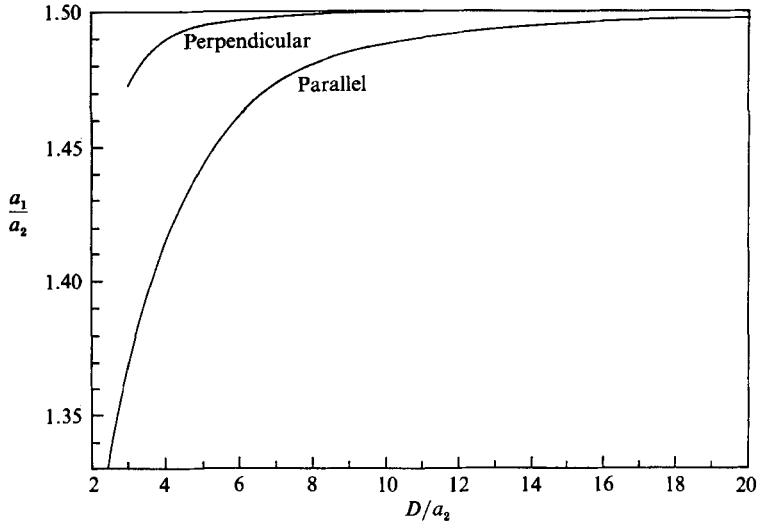

FIGURE 19. Plot of the ratio of the radii of the inner to outer spheres a_1/a_2 required for all three spheres in the chains shown in figure 18 to experience the same drag force as a function of interparticle spacing.

5. Symmetric multisphere configurations

Although the formulation in §2 is general enough to handle any three-dimensional configuration of a finite number of spherical particles, a considerable reduction in computation time and storage requirements may be realized by taking advantage of the symmetry of certain configurations.

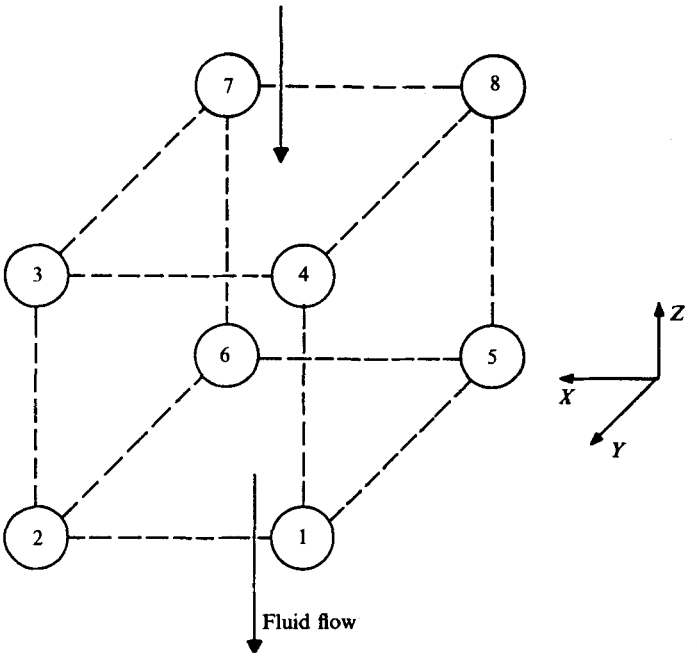

FIGURE 20. Eight rigidly held spheres in a simple cubic arrangement.

Accordingly, the general formulation outlined in §2 is modified to treat special cases of symmetric configurations as follows. The unknown constants introduced in (2.4) and the coefficients of these unknown constants shown in (2.18) and Appendix B are functions of the geometry and position of the spheres and the collocation rings with reference to the coordinate system shown in figure 1. In the case of a symmetric configuration of multiple spheres certain unknown constants (corresponding to a symmetric pair of spheres in the configuration) of the collocation series are equal in magnitude and either equal or opposite in sign depending upon the type of symmetry between the two spheres of the whole configuration with respect to the reference coordinate system. After doing numerous test runs involving all types of symmetric configurations, these unknown constants were identified as equal or opposite in sign for a pair of symmetric spheres according to their type of symmetry (see Appendix E).

For a system of J spheres in a given configuration, the first step in exploiting the symmetry conditions and reducing the number of equations and unknowns is to identify the type of symmetry between different pairs of spheres in that configuration. The two equations corresponding to a particular value of m' and a particular ring on a pair of symmetric spheres are added and subtracted. Depending on whether the unknown constants for that pair of symmetric spheres is equal or opposite for the particular symmetry (see Appendix E) only the non-zero coefficients of the unknown constants are retained. The set of equations for the other sphere are discarded. This reduces the number of equations by half and the coefficients in the collocation matrix by a factor of four. If the configuration is symmetric with respect to the X-, Y- and Z-planes then the number of equations is reduced by a factor of eight and the size of the collocation matrix by 64.

For a demonstration of this reduction technique, consider uniform flow past eight rigidly held spheres placed at the corner of a cube as shown in figure 20. This three-

dimensional multiparticle configuration of eight spheres is symmetric about the X-, Y- and Z-planes. The eight spheres are numbered as shown in figure 20 and a list of equal or opposite unknown constants for each pair of spheres is given below.

For symmetry about the Y-plane ($j = 1$ and 5, 2 and 6, 3 and 7, 4 and 8)

equal: $C_{j01}E_{j01}C_{j02}E_{j02}B_{j11}C_{j11}E_{j11}B_{j12}C_{j12}E_{j12}$

opposite: $A_{j01}A_{j02}A_{j11}D_{j11}F_{j11}A_{j12}D_{j12}F_{j12}$.

For symmetry about the Z-plane ($j = 1$ and 4, 2 and 3)

equal: $A_{j01}C_{j02}E_{j02}C_{j11}D_{j11}E_{j11}F_{j11}A_{j12}B_{j12}$

opposite: $C_{j01}E_{j01}A_{j02}A_{j11}B_{j11}C_{j12}D_{j12}F_{j12}$.

For symmetry about the X-plane ($j = 1$ and 4)

equal: $A_{j01}A_{j02}B_{j11}C_{j11}E_{j11}B_{j12}C_{j12}E_{j12}$

opposite: $C_{j01}E_{j01}C_{j02}E_{j02}A_{j11}D_{j11}F_{j11}A_{j12}D_{j12}F_{j12}$.

Spheres 1, 2, 3 and 4 are symmetric with spheres 5, 6, 7 and 8 respectively about the Y-plane. Hence for the set of equations for sphere 1 the coefficients of the unknown constants for sphere 1 are added and subtracted with that of sphere 5 and all the non-zero terms are retained in the set of equations for sphere1 while the set of equations for sphere 5 is no longer needed. A similar technique is used for the other three pairs of spheres (i.e. 2 and 4, 3 and 7, 4 and 8). This leaves only the set of equations for spheres 1, 2, 3 and 4. Then symmetry conditions about the Z-plane are used for sphere pairs (1, 4) and (2, 3). Here spheres 5, 6, 7 and 8 are not considered as the equations corresponding to them have already been accounted for when using the symmetry about the Y-plane. Coefficients for sphere 1 are added and subtracted with those of sphere 4 in the set of equations for sphere 1, retaining only the non-zero term in the set of equations for sphere 1 and discarding the set of equations for sphere 4. This is also done for the pair (2, 3). Now only the sets of equations for spheres 1 and 2 are left. Finally the symmetry about the X-plane is used between spheres 1 and 2 (as equations for all other spheres are eliminated using symmetry about the X- and Y-planes) and coefficients in the set of equations for sphere 1 are added and subtracted with those of sphere 2, retaining only the equations for sphere 1 with non-zero coefficients. This reduces the set of equations by a factor of eight and the matrix size by 64.

Using the symmetry theory described above, the drag force on symmetric configurations of 8, 16, 24, 32, 40, 48, 56 and 64 spheres were obtained. Results for two cases with different sphere configurations are presented. In the first case, the initial set of eight spheres were placed at the corners of a cube and then sets of eight spheres up to a total of 64 spheres were added to construct a $4 \times 4 \times 4$ cube around the initial cube. In the second case, the initial set of eight spheres were placed at the corners of a cube and then sets of eight spheres added in the direction of flow, enclosing the initial cube to form four columns of spheres. In both cases, the centre-to-centre spacing between any two adjacent spheres was 16.12 sphere radii corresponding to a particle concentration of 0.001. The values of the drag force F_z, non-dimensionalized by the drag force on an isolated sphere, on each of the eight spheres that make up the innermost cube are presented in figure 21 for increasing number of spheres J in the whole configuration. The drag force decreases with increasing number of spheres owing to the shielding effect of the outer spheres on the

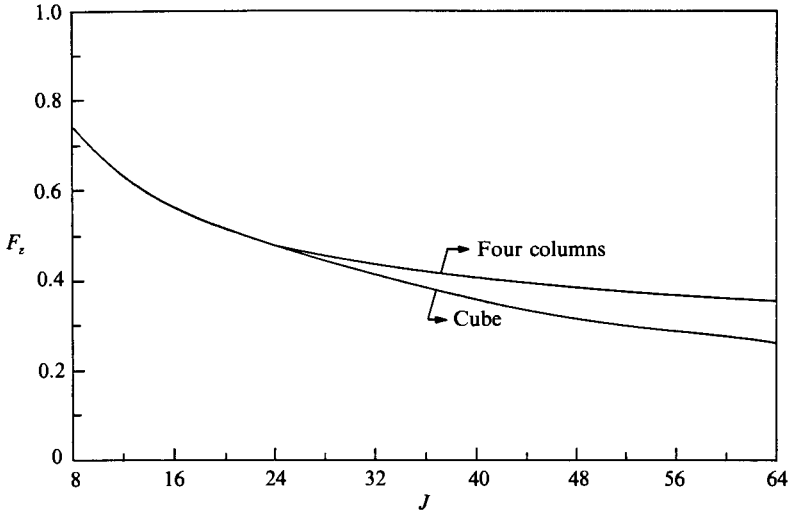

FIGURE 21. Drag force F_z on each of the four innermost spheres for increasing number of spheres J.

inner spheres in both cases, but the decrease in the drag for the first case is greater because the shielding of the innermost sphere is from all directions.

As a check for the present method, the drag force on 64 spheres rigidly held in place in a uniform flow at the corners of a $4 \times 4 \times 4$ simple cubic array (see figure 22) were compared with those obtained by the method of Durlofsky, Brady & Bossis (1987). For a centre-to-centre distance of 8.06 particle diameters we used two collocation rings on each sphere and retained the first two terms in the Fourier series. Our results of the drag force parallel to the direction of flow on each of 64 spheres matched with the results of Durlofsky, Brady & Bossis (1987) to at least four decimal places, and table 5 gives a comparison of the drag force on 64 spheres obtained by the method of Durlofsky *et al.* $F_{z,\mathrm{DBB}}$ and by the present method $F_{z,\mathrm{HGP}}$. The values of the force are presented for sets of eight spheres having symmetry about the X-, Y- and Z-planes.

6. Concluding remarks

The developed technique is extremely accurate in predicting the hydrodynamic interactions for a finite number of spheres arranged at any arbitrary configuration in three-dimensional space. It provides a general solution for velocity and pressure fields and can be used to calculate translational and rotational velocities, force and torque. In principle, the method can give any degree of numerical accuracy by simply increasing the number of collocation rings where the no-slip boundary conditions are satisfied on the surface of each sphere, and by increasing the number of terms retained in the Fourier series. The fluid velocity field, which is obtained accurately, can show any fine structure such as a closed circulation of fluid if it exists.

However, there has to be a compromise between the accuracy, number of spheres, the interparticle spacing and the computational time required. We have been able to accurately study fully three-dimensional configurations containing up to 32 spheres at a centre-to-centre spacing of 8 diameters and we also looked at configurations

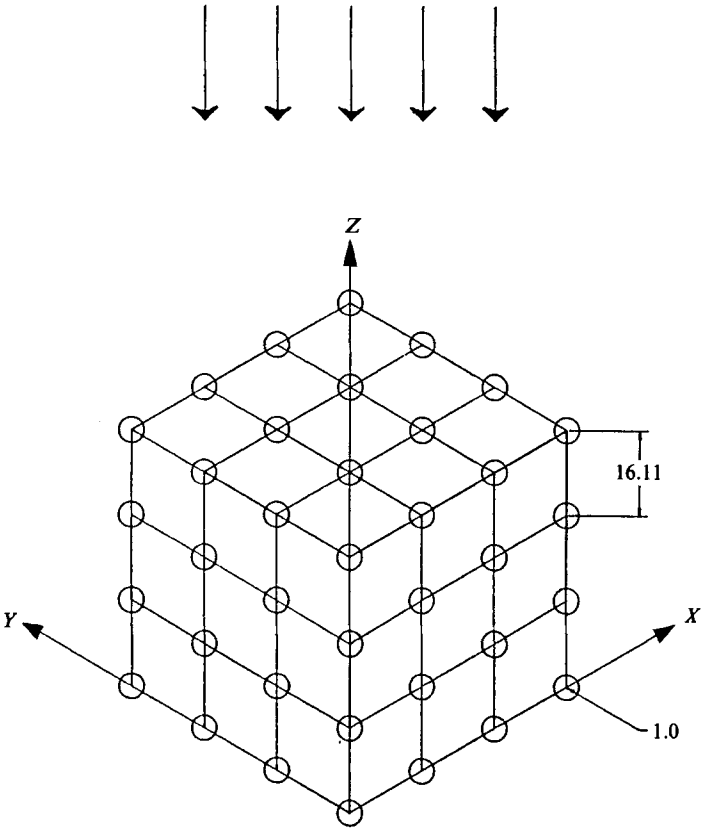

FIGURE 22. Schematic diagram of uniform flow past 64 identical spheres rigidly held in a simple cubic arrangement.

containing fewer spheres as close as 1.01 diameters. The computational time required for a single arbitrary three-dimensional asymmetric configuration of particles is approximately $3JN(2M-1)\times 0.05$ s on an IBM 3081 computer. Runs made on a CRAY II supercomputer at Research Equipment Inc. of the University of Minnesota utilizing the vectorization abilities of that processor required one third of the computational time cited above. This time is used primarily for the numerical evaluation of the integrals in the coefficient matrix. The storage requirement on the IBM 3081 is approximately $8/1024\times(3JN)^2(2M)(2M-1)$ K-bytes using double-precision arithmetic (16 digits). The computational time is the main drawback of this method, which can be overcome to a certain extent by using symmetry conditions for symmetric configurations.

When applying this method of solution to practical problems we should single out its major advantages and disadvantages compared to other methods of solution, particularly the approach of Durlofsky *et al.* (1987). The main advantages include the ability to obtain pointwise solutions. Fluid velocity and whole streamlines can be traced, thus enabling, in principle, tracing a fluid particle and other scalar quantities associated with it. The functions associated with particle motions, such as force, torque and stress, can in principle be evaluated accurately. These cannot be provided by the method of Durlofsky *et al.* (1987) which makes use of two-body interactions at close spacings and is only asymptotically correct at very high or very

Set no.	Position of the 8 spheres in the set symmetric about the X-, Y- & Z-planes	$F_{z,\mathrm{DBB}}$	$F_{z,\mathrm{HGP}}$
1	(0, 0, 0) (0, −16.1, 0) (0, 0, −16.1) (0, −16.1, −16.1) (−16.1, 0, 0) (−16.1, −16.1, 0) (−16.1, 0, −16.1) (−16.1, −16.1, −16.1)	0.2619	0.2619
2	(0, 0, 16.1) (0, −16.1, 16.1) (0, 0, −32.2) (0, −16.1, −32.2) (−16.1, 0, 16.1) (−16.1, −16.1, 16.1) (−16.1, 0, −32.2) (−16.1, −16.1, −32.2)	0.3198	0.3198
3	(16.1, 0, 0) (16.1, −16.1, 0) (16.1, 0, −16.1) (16.1, −16.1, −16.1) (−32.2, 0, 0) (−32.2, −16.1, 0) (−32.2, 0, −16.1) (−32.2, −16.1, −16.1)	0.3442	0.3442
4	(16.1, 0, 0) (16.1, −16.1, 0) (16.1, 0, −16.1) (16.1, −16.1, −16.1) (−32.2, 0, 0) (−32.2, −16.1, 0) (−32.2, 0, −16.1) (−32.2, −16.1, −16.1)	0.4006	0.4006
5	(0, 16.1, 0) (0, −32.2, 0) (0, 16.1, −16.1) (0, −32.2, −16.1) (−16.1, 16.1, 0) (−16.1, −32.2, 0) (−16.1, 16.1, −16.1) (−16.1, −32.2, −16.1)	0.3442	0.3442
6	(0, 16.1, 16.1) (0, −32.2, 16.1) (0, 16.1, −32.2) (0, −32.2, −32.2) (−16.1, 16.1, 16.1) (−16.1, −32.2, 16.1) (−16.1, 16.1, −32.2) (−16.1, −32.2, −32.2)	0.4006	0.4006
7	(16.1, 16.1, 0) (16.1, −32.2, 0) (16.1, 16.1, −16.1) (16.1, −32.2, −16.1) (−32.2, 16.1, 0) (−32.2, −32.2, 0) (−32.2, 16.1, −16.1) (−32.2, −32.2, −16.1)	0.4174	0.4174
8	(16.1, 16.1, 0) (16.1, −32.2, 0) (16.1, 16.1, −16.1) (16.1, −32.2, −16.1) (−32.2, 16.1, 0) (−32.2, −32.2, 0) (−32.2, 16.1, −16.1) (−32.2, −32.2, −16.1)	0.4700	0.4700

TABLE 5. Comparison of results for the drag force on 64 spheres rigidly held in a uniform flow at the corners of a $4 \times 4 \times 4$ simple cube. Centre-to-centre spacing between any two adjacent spheres is 16.12 sphere radii.

low particle proximities. The one major disadvantage is that the method uses large computer volumes and calculations take a long time. This disadvantage, which is not a serious drawback in Durlofsky *et al.* (1987), limits the application considerably.

In view of the computer space and time limitations, the possible applications must focus on the instantaneous exposure of particle configurations. Evaluation of a cloud of a few particles is feasible. Interaction between particles in a variable shear flow can also be accurately studied. The method can also be used to obtain streamlines in multiparticle arrays which form the basis for heat and mass transfer studies and evaluation of effective conductivities in suspension. A macroscopic property that is feasible to calculate is the so-called long-wave oscillatory viscosity. This kind of calculation does not necessarily require ensemble averaging of many realizations. It is also possible to do bounded flow problems accurately using this method.

This research was supported by NSF Creativity Grant CPE 85-00301 and by a grant from The City University of New York PSC-CUNY Research Award Program, No. 6-62036(FY-13). Their support is gratefully acknowledged. The authors wish to thank Professor A. Nir of the Technion-Israel Institute of Technology Israel for his help and suggestions during his visit to CCNY. The authors also wish to thank the City University of New York Computer Center and the City College of New York Computer Center for the use of their facilities and the National Science Foundation Office of Advanced Scientific Computing for providing access to the CRAY I and CRAY II supercomputer facilities at the University of Minnesota.

The above work has been performed in partial fulfilment of the requirements for the Ph.D. degree of Q. Hassonjee from The Graduate School of The City University of New York.

Appendices

Appendices A–E are not reproduced here. Copies of these appendices may be obtained either from the authors or from the Editor.

Appendix A. Derivation of coordinate transformations (2.7), (2.8) and (2.9).

Appendix B. Explicit expressions for the primed coefficients in (2.11).

Appendix C. Explicit expressions for the primed functions in (2.17).

Appendix D. Collocation matrix equation for two spheres with two rings and two terms retained in the Fourier series.

Appendix E. Symmetry classification of the unknown constants introduced in (2.4).

REFERENCES

DAVIS, A. M. J., O'NEILL, M. E., DORREPAAL, J. M. & RANGER, K. B. 1976 Separation from the surface of two equal spheres in Stokes flow. *J. Fluid Mech.* **77**, 625–644.

DAVIS, M. H. 1969 The slow translation and rotation of two unequal spheres in a viscous fluid. *Chem. Engng Sci.* **24**, 1769–1776.

DAGAN, Z., WEINBAUM, S. & PFEFFER, R. 1983 Theory and experiment on the three-dimensional motion of a freely suspended spherical particle at the entrance to a pore at low Reynolds number. *Chem. Engng Sci.* **38**, 583–596.

DEAN, W. R. & O'NEILL, M. E. 1963 A slow motion of viscous liquid caused by the rotation of a solid sphere. *Mathematica* **10**, 13–26.

DURLOFSKY, L., BRADY, J. F. & BOSSIS, G. 1987 Dynamic simulation of hydrodynamically interacting particles. *J. Fluid Mech.* **180**, 21–49.

GANATOS, P., PFEFFER, R. & WEINBAUM, S. 1978 A numerical-solution technique for three-dimensional Stokes flows, with application to the motion of strongly interacting spheres in a plane. *J. Fluid Mech.* **84**, 79–111.

GANATOS, P., WEINBAUM, S. & PFEFFER, R. 1980*a* A strong interaction theory for the creeping motion of a sphere between plane parallel boundaries. Part 1. Perpendicular motion. *J. Fluid Mech.* **99**, 739–753.

GANATOS, P., PFEFFER, R. & WEINBAUM, S. 1980*b* A strong interaction theory for the creeping motion of a sphere between plane parallel boundaries. Part 2. Parallel motion. *J. Fluid Mech.* **99**, 755–783.

GANATOS, P., WEINBAUM, S. & PFEFFER, R. 1982 Gravitational and zero-drag motion of a sphere of arbitrary size in an inclined channel at low Reynolds number. *J. Fluid Mech.* **124**, 27–43.

GLUCKMAN, M. J., PFEFFER, R. & WEINBAUM, S. 1971 A new technique for treating multiparticle slow viscous flow: axisymmetric flow past spheres and spheroids. *J. Fluid Mech.* **50**, 705–740.

GLUCKMAN, M. J., WEINBAUM, S. & PFEFFER, R. 1972 Axisymmetric slow viscous flow past an arbitrary convex body of revolution. *J. Fluid Mech.* **55**, 677–709.

GOLDMAN, A. J., COX, R. G. & BRENNER, H. 1966 The slow motion of two identical arbitrarily oriented spheres through a viscous fluid. *Chem. Engng Sci.* **21**, 1151–1170.

HAPPEL, J. & BRENNER, H. 1973 *Low Reynolds Number Hydrodynamics*, 2nd edn. Noordhoff.

HASIMOTO, M. 1959 On the periodic fundamental solutions of the Stokes equations and their application to viscous flow past a cubic array of spheres. *J. Fluid Mech.* **5**, 317–328.

HOCKING, L. M. 1964 The behaviour of clusters of spheres falling in a viscous fluid. Part 2. Slow motion theory. *J. Fluid Mech.* **20**, 129–139.

JAYAWEERA, K. O. L. F., MASON, B. J. & SLACK, G. W. 1964 The behaviour of clusters of spheres falling in a viscous fluid. Part 1. Experiment. *J. Fluid Mech.* **20**, 121–128.

KIM, S. & MIFFLIN, R. T. 1985 The resistance and mobility functions of two equal spheres in low-Reynolds-number flow. *Phys. Fluids* **28**, 2033–2045.

LAMB, H. 1945 *Hydrodynamics*, 6th edn. Dover.

LIAO, W. H. & KRUEGER, D. A. 1980 Multipole expansion calculation of slow viscous flow about spheroids of different sizes. *J. Fluid Mech.* **96**, 223–241.

SANGANI, A. S. & ACRIVOS, A. 1982 Slow flow through periodic arrays of spheres. *Intl J. Multiphase Flow* **8**, 343–360.

STIMSON, M. & JEFFERY, G. B. 1926 The motion of two spheres in a viscous fluid. *Proc. R. Soc. Lond.* A **111**, 110–116.

WACHOLDER, E. & SATHER, N. F. 1974 The hydrodynamic interaction of two unequal spheres moving under gravity through quiescent viscous fluid. *J. Fluid Mech.* **65**, 417–437.

WAKIYA, S. 1967 Slow motions of a viscous fluid around two spheres. *J. Phys. Soc. Japan* **22**, 1101–1109.

YAN, Z. Y., WEINBAUM, S., GANATOS, P. & PFEFFER, R. 1987 The three-dimensional hydrodynamic interaction of a finite sphere with a circular orifice at low Reynolds number. *J. Fluid Mech.* **174**, 39–68.

ZICK, A. A. & HOMSY, G. M. 1982 Stokes flow through periodic arrays of spheres. *J. Fluid Mech.* **115**, 13–26.